Speculative behaviour and complex asset price dynamics

Carl Chiarella (carl.chiarella@uts.edu.au)
School of Finance and Economics
University of Technology, Sydney

Roberto Dieci (dieci@economia.econ.unipr.it)
Facoltà di Economia
Università degli Studi di Parma

Laura Gardini (gardini@econ.uniurb.it)
Facoltà di Economia, Università degli Studi di Parma and
Università di Urbino

Abstract

This paper analyses the dynamics of a model of a share market consisting of two groups of traders: fundamentalists, who form rational expectations on the fundamental value of the asset, and chartists, who base their trading decisions on an analysis of past price trends. The model is reduced to a two-dimensional map whose dynamic behaviour is analysed in detail, particularly with respect to global dynamical behaviour. The dynamics are a®ected by parameters measuring the strength of fundamentalist demand and the speed with which chartists adjust their estimate of the trend to past price changes. The parameter space is characterized according to the local stability/instability of the equilibrium point as well as the noninvertibility of the map. The method of critical curves of noninvertible maps is used to understand and describe the range of global bifurcations that can occur. It is also shown how the knowledge of deterministic dynamics uncovered here can aid in understanding stochastic versions of the model.

1 Introduction

In recent years several models of financial markets based on interacting heterogeneous agents have been developed, see for example [3], [18], [4] and [7]. These models, which generally allow the size of the different groups of agents to vary according to the evolution of the financial market, are of necessity not very mathematically tractable. In the present paper, in order to complement the above mentioned studies, we shall present a model containing the essential elements of the heterogeneous interacting agents paradigm whilst still remaining mathematically tractable. The model that we shall develop is a discrete time model of asset price dynamics, which includes as a particular case the one presented in [5] and considered in more detail in [12]. We shall assume that the share market consists of two types of traders: fundamentalists, who are forming rational expectations on the fundamental value of the asset, and chartists, a group which bases its trading decisions on an analysis of past price trends. The chartists' demand is assumed to be an S-shaped function of the difference between the chartists' estimate of the price trend (obtained through an adaptive expectations scheme on past price changes) and the return on some alternative asset. The model is reduced to a two-dimensional nonlinear map. To investigate the dynamic behaviour of the model we shall first determine, in the space of the parameters, the local stability region of the unique equilibrium point of the map, together with the regions of invertibility or non invertibility. It will appear that also in the stability region, besides the local properties, global ones are important in order to detect other dynamic phenomena such as coexistence of attractors, chaotic transients before the convergence to the stable equilibrium, or divergence of points very close to the stable equilibrium.

We shall indicate the bifurcations that the fixed point undergoes when the key parameters, such as the strength of fundamentalists' demand and the speed with which chartists adjust their estimate of the trend to past price changes, are increased. We shall also analyze the regions in the parameter space in which the equilibrium point is unstable and the map is noninvertible. We shall focus on particular regimes characterized by chaotic behaviour, showing how the global bifurcation known as snap-back repellor (leading to chaotic dynamics) can be detected by use of the critical curves of the map (as proved in [13]). Moreover, by making use of the properties of the critical curves of noninvertible maps (described in Chapter 4 of [20], and already

used in several economic models, see e.g. [21]), we shall show how upper and lower bounds for the asymptotic behaviour of the state variables (price and chartists' expectations) can be determined, although we are in the presence of chaotic dynamics.

The paper is organized as follows. Section 2 derives our model of fundamentalists and chartists. Section 3 points out some general properties of the two-dimensional map driving the dynamics. Sections 4 contains numerical simulations and in Section 5 we show how the properties of the critical curves can help to understand the nature of the attractors, their homoclinic bifurcations and other global bifurcations. Finally, an extension of the model beyond its deterministic structure is suggested in Section 6, showing how the knowledge of deterministic dynamics can help in the understanding of simple stochastic models. Section 7 concludes and makes some suggestions for future research.

2 The model

We adopt the basic fundamentalist/chartist model of [5], whose antecedents are [2] and [22]. Let us denote by P_t the logarithm of the asset price at time t. Excess demand for the asset at time t (D_t) is composed of fundamentalist demand (D_t^0) and chartist demand (d_t), i.e.:

$$D_t = D_t^0 + d_t \quad .$$

The fundamentalists are assumed to have a reasonable knowledge of the fundamental value of the risky asset. This knowledge has been obtained at some cost, such as large setup costs (e.g. a major financial institution), and the employment of highly paid professionals, such as market analysts, economists, computer analysts, etc.. Fundamentalist demand is given by:

$$D_t^0 = a(W_t - P_t) \ , \tag{1}$$

where W_t is the logarithm of the fundamental value at time t and a ($a > 0$) is the strength of fundamentalist demand: if the share price P_t is below the rationally expected fundamental value W_t, then fundamentalists try to buy the share, because they think that the share is undervalued and therefore its price will increase, and vice versa; if P_t is above W_t, they try to sell, thinking that

the share is overvalued. The demand function of the fundamentalists could be derived in a one-period mean-variance optimizing framework in which fundamentalists have an exponential utility of wealth function. In such a framework demand for the risky asset is proportional to the fundamentalists' expectation of excess return on the risky asset divided by their risk-aversion coefficient and their estimate of the variance of the price change. The fundamentalists expect that (on average) the excess return will be proportional to the difference between W_t and P_t, and they also assume that the variance of price changes is constant. Thus the coefficient a is inversely proportional to the product of the risk-aversion coefficient and variance estimate of the fundamentalists. The technical details of the derivation of (1) within a utility maximising framework are given in the Appendix.

Chartists are assumed to be unable to bear the cost structure necessary to acquire the information about the fundamental value available to fundamentalists. Rather they base their investment decision on the costless information contained in recent price changes. Chartist demand is assumed to be a nonlinear increasing function of the anticipated return differential $(\tilde{A}_{t;t+1} \; ¡ \; g_t)$, where $\tilde{A}_{t;t+1}$ is the chartists' expectation at time t of the price change (i.e. return) over the next trading period, i.e.:

$$\tilde{A}_{t;t+1} = E_t\left[P_{t+1} \; ¡ \; P_t\right] = E_t\left[P_{t+1}\right] \; ¡ \; P_t$$

and g_t is the return on the alternative asset (e.g. bonds) over the same period. In particular we write:

$$d_t = h(\tilde{A}_{t;t+1} \; ¡ \; g_t) \; , \tag{2}$$

where the function $h(:)$ has the properties: (i) $h^{0}(x) > 0 \;\; (8x)$, (ii) $h(0) = 0$, (iii) there exists an $x^{¤}$ such that $h^{00}(x) < 0 \;\; (> 0)$ for all $x > x^{¤} \;\; (< x^{¤})$ and, (iv) $\lim_{x \, ! \, ¡ \, 1} h^{0}(x) = 0$.

The economic scenario behind the demand function h is also one in which chartists are one-period mean-variance maximisers with exponential utility of wealth functions. Their demand function will have the same general form as that of the fundamentalists. They differ from the fundamentalists in the way in which they calculate the expected excess return on the risky asset. Having less knowledge of the market they estimate return on the risky asset by extrapolating past returns according to (3) below. Furthermore their estimate of the variance of returns increases if they observe large excess

returns in the recent past, which explains the changing slope of the function h. Technical details of the derivation of chartist demand are also given in the Appendix.

A possible choice for the function $h(:)$ is:

$$h(x) = ® \arctan x \ ,$$

and this is the one used in our examples and simulations. However, it is important to remark that the qualitative analysis performed in the following sections (as also the qualitative dynamics) are not affected by a change of function, because these mainly depend on the properties of $h(:)$ given above. For example, a different demand function satisfying the same properties is considered in [12].

We assume that chartists form their expectation of the price change according to the simple adaptive scheme:

$$\tilde{A}_{t;t+1} = \tilde{A}_{t\,¡\,1;t} + c\,[P_t \ ¡ \ P_{t\,¡\,1} \ ¡ \ \tilde{A}_{t\,¡\,1;t}] \ , \tag{3}$$

where c $(0 < c \cdot 1)$ is the speed with which they adjust their estimate of the trend to the most recent price changes. Alternatively the quantity $¿ = 1=c$ may be viewed as the time lag in chartists' information[1].

Thus total excess demand for the asset at time t (assuming $g_t = g$ and $W_t = W$ are both constant) is given by:

$$D_t = a(W \ ¡ \ P_t) + h(\tilde{A}_{t;t+1} \ ¡ \ g) \ . \tag{4}$$

Let us now turn to the adjustment process of the share price in the market. We assume the existence of a market maker whose function is to set excess demand to zero at the end of each trading day by performing transactions at prices which differ from the market clearing values[2]. If the excess demand in period t is positive (negative), the market maker sells (buys) the quantity of the asset needed to clear the market, and raises (reduces) the share price for the next period $t+1$. Precisely, what goes on in each trading day can be described as follows.

[1] The restriction $c \cdot 1$, i.e. $¿ \ ¸ \ 1$, has the simple economic interpretation that chartists cannot revise their estimate of $\tilde{A}_{t;t+1}$ more frequently than they receive information about price changes. Here this frequency is one time unit.

[2] The role of the market maker and the impact of its behaviour on price dynamics are discussed, for example, in [14].

- At the beginning of day t the market maker announces the price P_t for that day.
- The market participants then form their demands, which generally will result in either positive or negative excess demand. More precisely, chartists compute $\tilde{A}_{t;t+1}$ according to (3) and both chartists and fundamentalists calculate their demands, resulting in excess demand D_t given by (4).
- The market maker, observing the excess demand, takes a long or short position M_t (by adjusting his/her inventory of assets) in order to clear the market, i.e. such that:

$$D_t + M_t = 0 \ .$$

- The market maker then announces, at the beginning of the next trading period, the price P_{t+1}. The new price is calculated as the previous price plus some fraction of the excess demand of the previous period according to:

$$P_{t+1} = P_t + \bar{\ }_p D_t \ .$$

  The process then repeats itself[3].

Thus at the beginning of day $(t+1)$ the following dynamic adjustments occur, made by the market maker and chartists, respectively:

$$\begin{cases} P_{t+1} = P_t + \bar{\ }_p \left[a(W - P_t) + h(\tilde{A}_{t;t+1} - g)\right] \\ \tilde{A}_{t+1;t+2} = (1 - c)\tilde{A}_{t;t+1} + c\bar{\ }_p \left[a(W - P_t) + h(\tilde{A}_{t;t+1} - g)\right] \end{cases} \tag{5}$$

It is worth noting that the model developed in the present section includes, as a particular case, the one obtained in [5], starting from different assumptions about the chartists' behaviour. Moreover the same dynamical system can be obtained following a different approach, as shown in [6]. These facts enhance the value of the model and increase the importance of its analysis.

[3] In order to remain mathematically tractable our model does not take into account the possible large positive or negative inventory positions of the market maker. These could be taken into account in the way the market maker adjusts the new price. We leave such analysis to future research.

In the present paper we are interested in showing how, in the regions of the parameters space where the equilibrium point is unstable, a different attractor exists having "good" properties from an applied point of view. That is, even if the fixed point of the system is unstable, we can predict the "fate" in a macroscopic way giving, for example, the width of the oscillations that the state variables such as P_t can undergo. To do this we shall make use of the properties of the critical lines, whose equation will be obtained in the next section, together with the stability region for the fixed point in the space of parameters.

3 Some general properties

3.1 The map

As described in the previous section, the time evolution of price and chartists' expectations is obtained by the iteration of a two-dimensional nonlinear map $Q : (\tilde{A}; P) \to (\tilde{A}'; P')$ given by:

$$Q : \begin{cases} \tilde{A}' = (1 - c)\tilde{A} + c\bar{}_p\,[a(W - P) + h(\tilde{A} - g)] \\ P' = P + \bar{}_p\,[a(W - P) + h(\tilde{A} - g)] \end{cases} , \qquad (6)$$

where the symbol $'$ denotes the unit time advancement operator. It can be easily checked that the map Q has the point $(\overline{\tilde{A}}; \overline{P}) = (0; W + 1/a\, h(-g))$ as unique fixed point. This implies that in equilibrium fundamentalist demand is $-h(-g)$ (> 0) and chartist demand is $h(-g)$ (< 0) i.e. in equilibrium fundamentalists are net buyers (since the price is below their estimated long run mean) and chartists are net sellers. Of course this situation can not be considered a true equilibrium situation, it is a result of the fact that our dynamic model is in fact a partial one in that it leaves in the background the market for the alternative asset. A general analysis needs to take into account the dynamics of the alternative asset. Then $(\tilde{A} - g)$ would be replaced by a single quantity, $'$ say, which would be the chartists expectation of the difference in price change of both asset prices. We would then be dealing with a three-dimensional dynamical system, at whose steady state it turns out that $' = 0$ and $\overline{P} = W$. Our analysis should thus be seen as that of a two-dimensional projection of this (more difficult to analyse) three-dimensional

system. For more details of the full three-dimensional system and some preliminary analysis of its dynamics we refer the reader to [8].

By introducing the price deviation $p = P - \overline{P}$ we obtain the new map $T : (\tilde{A}; p) \to (\tilde{A}'; p')$ given by:

$$T : \begin{cases} \tilde{A}' = (1 - c)\tilde{A} - c\bar{}_p [ap - k(\tilde{A})] \\ p' = p - \bar{}_p [ap - k(\tilde{A})] \end{cases}, \tag{7}$$

where

$$k(\tilde{A}) = h(\tilde{A} + g) - h(-g),$$

having the origin $O = (0; 0)$ as unique fixed point.

3.2 Local stability conditions

The local stability analysis of the fixed point O is performed via the evaluation of the two eigenvalues of the Jacobian matrix of the map[4] T:

$$DT(\tilde{A}; p) = \begin{bmatrix} 1 - c + c\bar{}_p \frac{\alpha}{1+(\tilde{A}+g)^2} & -ac\bar{}_p \\ -\bar{}_p \frac{\alpha}{1+(\tilde{A}+g)^2} & 1 - a\bar{}_p \end{bmatrix},$$

at $(0; 0)$. Let us denote by Tr and Det the trace and the determinant of $DT(0; 0)$ respectively, and by $P(z) = z^2 - Tr\, z + Det$ the associated characteristic polynomial. As it is well known a sufficient condition for the local stability consists in the following system of inequalities:

$$\begin{cases} P(1) = 1 - Tr + Det > 0 \\ P(-1) = 1 + Tr + Det > 0 \\ P(0) = Det < 1 \end{cases}, \tag{8}$$

giving necessary and sufficient condition for the two roots of the characteristic equation $P(z) = 0$ to be inside the unit circle of the complex plane (see, for instance, [15], p. 159). Elementary computations show that for our map the conditions (8) can be rewritten as:

$$\begin{cases} a\bar{}_p(2 - c) < 2(2 - c) + 2c\bar{}_p k'(0) \\ a\bar{}_p(1 - c) > c\,[\bar{}_p k'(0) - 1] \end{cases}. \tag{9}$$

[4] Note that for the assumed functional form of h, $k'(\tilde{A}) = \alpha/[1 + (\tilde{A} - g)^2]$.

Fig. 1 represents the region of local stability of the origin in the parameter plane $(c; a)$, $0 < c \cdot 1$, $a > 0$. From (9) it follows that, starting from parameters $(c; a)$ inside the stability region, a loss of stability may occur either via a flip bifurcation, when crossing the curve

$$a = \frac{2}{\bar{\rho}} + \frac{2ck^{0}(0)}{2 - c} , \qquad \text{(Flip-curve)} \tag{10}$$

or via a Neimark-Hopf bifurcation, when crossing the curve

$$a = \frac{c\,[\bar{\rho}k^{0}(0) - 1]}{\bar{\rho}(1 - c)} . \qquad \text{(Hopf-curve)} \tag{11}$$

By assuming $\bar{\rho} > 0$ as fixed, we notice that the shape of the stability region in the parameter plane $(c; a)$, indicated in dark grey in Fig. 1, is greatly affected by the strength of chartists' demand at the steady state $(k^{0}(0))$[5]. In particular, when $\bar{\rho}k^{0}(0) \cdot 1$ (Fig. 1a) the region appears wider than in the opposite case (Fig. 1b). Fig. 1a shows that, when strength of chartist demand is relatively weak $(k^{0}(0) < 1/\bar{\rho})$, at a given level of chartists reaction speed (c) the equilibrium is stable for sufficiently low values of the fundamentalists reaction parameter a, but fundamentalists can cause instability by reacting too strongly to the deviation from the fundamental value. Fig. 1b shows that when strength of chartist demand is relatively strong $(k^{0}(0) > 1/\bar{\rho})$, the ability of fundamentalists' demand to stabilise the system is restricted to a fairly narrow range of the parameter a.

INSERT FIG. 1 APPROXIMATELY HERE

3.3 Invertibility of the map

Let us now consider the invertibility conditions of the map. For particular values of the parameters, the map T is a noninvertible map of the plane. This means that, while starting from some initial values for asset price and chartists' expectations (say $(\tilde{A}_{0;1}; p_0)$) the iteration of (7) uniquely defines the trajectory $(\tilde{A}_{t;t+1}; p_t) = T^{t}(\tilde{A}_{0;1}; p_0)$ $(t = 1; 2; :::)$, the backward iteration

[5] We recall that for the particular chartist demand function that we have chosen, we have: $k^{0}(0) = ®/(1 + g^{2})$.

of (7) is not uniquely defined. In fact, a point $(\tilde{A};p)$ of the plane may have several rank-1 preimages[6].

Let us assume:

$$h(:) = \mathbb{R}\arctan(:) \qquad (\mathbb{R} > 0) \ ,$$

so that

$$k(\tilde{A}) = \mathbb{R}\arctan(\tilde{A} \ ¡ \ g) \ ¡ \ \mathbb{R}\arctan(\ ¡ g) \ .$$

It can be shown by elementary geometrical arguments that, by defining:

$$m = (a^{-}_{p} \ ¡ \ 1)\frac{(1 \ ¡ \ c)}{c} \ , \tag{12}$$

the map has a unique inverse for $m \cdot 0$ or $m \ ¸ \ \mathbb{R}^{-}_{p}$, while for $0 < m < \mathbb{R}^{-}_{p}$ the map is noninvertible. In particular, by defining:

$$\tilde{A}_1 = g \ ¡ \ \sqrt{\frac{\mathbb{R}^{-}_{p}}{m} \ ¡ \ 1}, \quad q_1 = {}^{-}_{p}k(\tilde{A}_1) \ ¡ \ m\tilde{A}_1 \tag{13}$$

$$\tilde{A}_2 = g + \sqrt{\frac{\mathbb{R}^{-}_{p}}{m} \ ¡ \ 1}, \quad q_2 = {}^{-}_{p}k(\tilde{A}_2) \ ¡ \ m\tilde{A}_2 \tag{14}$$

the points $(\tilde{A};p)$ of the phase plane for which the function $q = q(\tilde{A};p)$ defined by:

$$q(\tilde{A};p) = a^{-}_{p}p \ ¡ \ \frac{a^{-}_{p} \ ¡ \ 1}{c}\tilde{A} \ , \tag{15}$$

satisfies $q(\tilde{A};p) < q_1$ or $q(\tilde{A};p) > q_2$ have a unique rank-1 preimage, while the points for which: $q_1 < q(\tilde{A};p) < q_2$ have three distinct rank-1 preimages. Thus, following the notation used in [20], for $0 < m < \mathbb{R}^{-}_{p}$ this map is of the type $Z_1 \ ¡ \ Z_3 \ ¡ \ Z_1$, which means that the phase plane is subdivided into different regions Z_j $(j = 1;3)$, each point of which has j distinct rank-1 preimages. Such regions are bounded by the so-called critical curves of rank-1, defined as the locus of points having at least two merging rank-1 preimages (see [15]). For our map this set is defined as follows:

$$LC = \left\{ (\tilde{A};p) \ 2 \ R^2 : q(\tilde{A};p) = q_1 \ [\ q(\tilde{A};p) = q_2 \right\} \tag{16}$$

[6]Given a n-dimensional map $F : R^n \ ! \ R^n$ and a positive integer r we say that the point y is a rank-r preimage of the point x if $F^r(y) = x$, i.e. if y is mapped into x in r iterations.

where q_1 and q_2 are given in (13) and (14) respectively, and it is therefore made up of two straight lines, say $LC = L \cup L^0$, where L and L^0 have the equations:

$$L: \qquad p = \frac{a_p - 1}{a_p c}\tilde{A} + \frac{q_1}{a_p}\ ; \tag{17}$$

$$L^0: \qquad p = \frac{a_p - 1}{a_p c}\tilde{A} + \frac{q_2}{a_p}\ . \tag{18}$$

Each of the critical points $(\tilde{A}; p) \in LC$ has two merging rank-1 preimages, and the locus of such preimages, denoted by LC_{-1} (this defines the critical curve of rank-0), turns out to be made up of two straight lines, say $LC_{-1} = L_{-1} \cup L^0_{-1}$, whose equations are:

$$L_{-1}: \qquad \tilde{A} = g - \sqrt{\frac{\beta_p}{m}} - 1\ ; \tag{19}$$

$$L^0_{-1}: \qquad \tilde{A} = g + \sqrt{\frac{\beta_p}{m}} - 1\ , \tag{20}$$

The critical curve LC_{-1} corresponds here to the locus of points $(\tilde{A}; p)$ of the phase plane in which the determinant of the Jacobian matrix $DT(\tilde{A}; p)$ vanishes[7].

Also the images of this set are called critical curves of higher rank. The curves:

$$LC_k = T^k(LC) = T^{k+1}(LC_{-1}) \qquad \text{for } k = 0; 1; 2; ...$$

are called critical curves of rank-$(k+1)$ ($LC_0 = LC$): In our example we always have two branches:

$$LC_k = L_k \cup L^0_k = T^{k+1}(L_{-1}) \cup T^{k+1}(L^0_{-1}).$$

In order to compare the bifurcation curves in the parameter plane $(c; a)$ with the ranges of invertibility or non invertibility of the map T, it is useful to draw in the same $(c; a)$ plane the region in which the noninvertibility condition $0 < m < \beta_p$ is fulfilled.

[7] Generally speaking, for a differentiable map the critical curve LC_{-1} is a subset of the locus of points of the phase plane for which the determinant of the Jacobian matrix of the map vanishes.

Taking into account eq. (12), the condition $m > 0$ can be rewritten as:

$$\begin{cases} 0 < c < 1 \\ a > 1/\bar{p} \end{cases},$$

while the condition $m < \beta/\bar{p}$, becomes:

$$\begin{cases} 0 < c < 1 \\ a < \beta c/(1-c) + 1/\bar{p} \end{cases}.$$

The noninvertibility region of the map T is indicated in light grey in Fig. 1. It is worth noting that the higher is the value of β, i.e. the strength of chartist demand at the steady state $k^0(0)$, the wider is the noninvertibility region. Moreover we can see that in the region defined by

$$\begin{cases} 0 < c < 1 \\ a < 1/\bar{p} \end{cases},$$

the map is invertible no matter what the value of $k^0(0)$ is.

In the next section we shall investigate the dynamics of the map in different regions of the parameters space, mainly in order to highlight the impact, on the dynamics, of the parameter c, measuring the speed of adjustment of chartists' expectations. To do this we will focus, in particular, on the case $\bar{p}k^0(0) > 1$ (i.e. strength of chartist demand is relatively strong) in which, as we can see from Fig. 1b, the equilibrium "soon" becomes unstable as the parameter c is increased.

4 Flip and Hopf bifurcations and related global bifurcations in attracting sets

The purpose of this section is to describe some of the possible types of dynamical behaviour of the model (5) when the parameters are allowed to vary both within the stability region for the equilibrium point O and out beyond that region, crossing either the Flip-curve or the Hopf-curve. As already remarked in Section 3, assuming the parameter c in the interval $(0;1)$, we have to consider two cases, qualitatively represented in Fig. 1. That is, if the parameters satisfy $\bar{p}k^0(0) < 1$(i.e. chartist demand is relatively weak), then we

have a wide stability region (Fig. 1a) which includes any value $c \in (0;1)$ for sufficiently low values of the parameter a, and stability is lost only via a Flip bifurcation as the strength of fundamentalist demand a is increased. While when $\bar{}_p k^{\prime}(0) > 1$ (i.e. chartist demand is relatively strong) the stability region is reduced (Fig. 1b) and at low values of a the fixed point undergoes a Neimark-Hopf bifurcation, while the Flip-curve still exists for high values of a. It has been observed numerically that the crossing of the Flip-curve yields the same qualitative dynamics, independently of $\bar{}_p k^{\prime}(0) < 1$ (Fig. 1a) or $\bar{}_p k^{\prime}(0) > 1$(Fig. 1b). Hence in this section we shall consider, without loss of generality, only examples of the second kind.

4.1 Stability region

Let us assume $\bar{}_p = 2{:}6$, $g = 1$ and $® = 2{:}5$ so that $\bar{}_p k^{\prime}(0) = 3{:}25 > 1$, and consider a point belonging to the stability region. Fig. 2a shows a trajectory in the phase-plane which spirals around the attracting focus O, while Fig. 2b shows the values of the price deviation p as a function of time. In this example the basin of attraction of O, say $B(O)$, which is the locus of points whose trajectories converge to the stable equilibrium, is a fairly wide region of the phase-plane. However, it is worth noting that for different values of the parameters c and a, always inside the stability region represented in Fig. 1b, we shall observe via the examples in this section several other dynamic phenomena. That is, besides the attracting fixed point O, in the region of the phase-plane of interest for applications we may have also

(i) a coexisting attractor (regular or chaotic),

(ii) points having divergent trajectories,

(iii) a chaotic repellor.

In case (i) we shall denote by A the coexisting attractor, and by $B(A)$ its basin of attraction which, as we shall see, may also be wider than $B(O)$. Case (ii) is quite common in nonlinear maps, but we are interested to see if such points are close to the attractors or far away from them. Such points, which are not meaningful in a practical sense, may be viewed as points converging to an attractor at infinity, on the "Poincaré equator", i.e. an improper

point of the phase-plane. We shall denote by $\mathsf{B}(\,\mathsf{1}\,)$ the set of points having divergent trajectories (basin of attraction of a point at infinity). The complementary set in the phase-plane is the set of points having bounded trajectories. As noticed in case (i) above, this set may be shared between two or more coexisting attracting sets.

An example is given in Fig. 2c where besides the stable focus O there exists a coexisting attracting 4-cycle A_4. The white region denotes the closure of the basin $\mathsf{B}(\mathsf{O})$ while the closure of the basin $\mathsf{B}(\mathsf{A}_4)$ is in light grey. A third attractor is at infinity, and the basin $\mathsf{B}(\,\mathsf{1}\,)$ is the dark grey region. It is clear that in similar cases, although the unique fixed point of the system is locally stable, we must be careful in saying that the system approaches the attracting equilibrium, because the time evolution strongly depends on the initial state.

It is important to evaluate also the "robustness" of the stability property with respect to external events, or shocks, which abruptly modify the state of the system, moving the point away from its "true" state. For example we can certainly say that the stability of the fixed point O in the case shown in Fig. 2a is robust with respect to external perturbations. In fact, given any initial condition in that region, its trajectory converges towards the stable focus and even if, at a given time, a shock moves the point in the phase-plane, we simply get another initial condition in the same basin and thus the effect of the shock is simply a slight change in the oscillatory motion converging to the fixed point.

This is no longer true in the case shown in Fig. 2c. In fact, even if we start from an initial condition in $\mathsf{B}(\mathsf{O})$, a shock may bring the phase-point inside a different basin of attraction, thus changing the asymptotic behaviour of the trajectory. We may ultimately converge to the attracting cycle of period 4 or even diverge. In Fig. 2d the trajectories of two nearby initial conditions are shown: one gives damped oscillations towards O, while the other gives wide oscillations converging to the 4-cycle.

It is important to note that in the case of a noninvertible map, as it is in this regime, the basins of attraction of coexisting attracting sets are generally not connected (a property which cannot occur in invertible maps). It is evident that the basin (in grey) of the 4-cycle in Fig. 2c is non connected. The reason why the basins have such a structure is that the total basin is obtained by taking all the preimages of any rank of the "immediate basin". Precisely, the immediate basin of the 4-cycle is obtained by considering the

4 fixed points of the map T^4, for each of them we take the widest simply connected area contained in the basin, including the periodic points. The immediate basin B_0 of the 4-cycle of T is the union of 4 disjoint, cyclical areas[8]. Then the whole basin is $B = [_{n,0} T^{-n}(B_0)$, and we get the light grey area shown in Fig. 2c.

But the complementary set of $B(1)$ may also display a different structure. Instead of coexisting attractors (which may also be the stable fixed point O and a chaotic attractor), we may have coexistence of the stable fixed point with a strange repellor, as already remarked in (iii). The presence of such an "invisible chaos" can be deduced from the transient part of the trajectory. An example is shown in Fig. 2e. There the grey region denotes $B(1)$ while the white region gives the closure of the basin $B(O)$. This means that any point in the white region, except for a set Λ of zero Lebesgue measure, has a trajectory converging to O. However, we may observe a very strange behaviour in the transient part of the state values. Compare the points of the trajectory in the cases shown in Fig. 2a and Fig. 2e and the corresponding representations of the state variable p as a function of time (Figs. 2b and 2f, respectively). It is clear that if we restrict our interest to a "short period", as it is often the case in applications, then it is difficult to "classify" the robustness of the stability of O. In the case of Fig. 2e the dynamic behaviour in the short time is the same as the one observed when O is unstable and a chaotic attractor exists around it (as we shall see again later). Thus, looking at the transient part we cannot predict if the system is stable or unstable, i.e. whether the state will ultimately settle in the stable fixed point or if it will wander chaotically, and unpredictably, around it.

INSERT FIG. 2 APPROXIMATELY HERE

We may ask how such a chaotic repellor, Λ, was created. It is invariant for the map T, i.e. $T(\Lambda) = \Lambda$, and the restriction of T to Λ is a map with chaotic behaviour. Even if Λ is a set of zero Lebesgue measure, it is homeomorphic to a Cantor set. As it is not embedded into an absorbing area, it behaves like a "chaotic saddle" or "invisible chaos". Its formation is often due to a sequence of flip bifurcations of saddles. It is well known nowadays that one of the most common routes to chaos is associated with the so-called "flip sequence" or "period doubling sequence". In the two-dimensional case

[8] That is the four grey areas in Fig. 2c containing the points x_1, x_2, x_3 and x_4.

such a mechanism may have two different effects depending on the nature of the starting cycle, which may be a stable node or a saddle. For example, starting from a stable node one of the two eigenvalues may cross through the value ¡1, leaving the cycle as saddle and giving rise to an attracting node of double period. This process may be repeated indefinitely, often leading to a chaotic attractor. In the same way, starting from a saddle cycle, the second eigenvalue may cross the value ¡1 and the resulting flip bifurcation changes the saddle into a repelling node giving rise to a saddle cycle of double period, and so on. Such a sequence of "invisible" flip bifurcations, applied to unstable cycles and creating unstable cycles, is often the mechanism which gives rise to a chaotic repellor Λ. The set Λ includes all the infinitely many saddles and unstable nodes created along the "route" together with all their stable sets. We remark that in the case of non invertible maps (as it is the case of our model for values of the parameters in the light grey regions in Figs. 1a and 1b), also the unstable nodes and unstable foci have a stable set, given by all the preimages of any rank of the periodic points, and in our examples these preimages may be infinitely many. Moreover, as we shall see in Section 5, the existence of preimages of repelling nodes or foci gives one of the simplest ways to detect the chaotic behaviour of the system ("visible" or "invisible"), which is otherwise difficult to prove. We have seen above that a stable fixed point may be considered as "practically unstable" because of a very small basin of attraction. We notice that this may occur also when the fixed point is the only attractor and no other cycles exist, neither stable nor unstable, except for a finite number of saddles on the boundary of its basin. An example is shown in Fig. 3a, where the basin B(1) is close to the fixed point O, which is an attracting node. Thus, two nearby initial conditions, even very close to O, may lead to very different dynamic behaviour, as shown in Fig. 3b, where in one case the state variable p approaches its equilibrium value, and in the other case it takes increasing values with a catastrophic effect.

INSERT FIG. 3 APPROXIMATELY HERE

4.2 Crossing the Neimark-Hopf bifurcation curve

We are now interested in the description of the types of dynamic behaviour that may occur when the fixed point becomes unstable via a crossing of the

Neimark-Hopf bifurcation curve. As we shall see, starting from inside the stability region of Fig. 1b with a value of a sufficiently high, an increase of the parameter c leads to oscillatory behaviour which may become chaotic around O, and as c approaches the value 1 the dominating state is an attracting cycle (although coexisting with a strange repellor) with a wide basin of attraction. While when the same Hopf-curve is crossed at low values of the parameter a, we have numerically observed a stronger "stability effect", with persistence of regular oscillations.

Let us fix a = 0:8 and increase the parameter c. When crossing the Neimark-Hopf bifurcation curve we observe a supercritical bifurcation, leaving a repelling focus O surrounded by an attracting closed invariant curve, see Γ in Fig. 4a, on which the trajectories are either periodic (when the rotation number at the Neimark-Hopf bifurcation is rational) or quasi-periodic (when the rotation number is irrational), as described in [16].

In Section 5 we shall see the effects of the noninvertibility of the map, which shall lead us to the construction of an absorbing area inside which the attractors are confined. Now we simply observe that local and global bifurcations occurring to the attracting set existing around O give rise to a chaotic attractor A of "annular shape", as the one shown in Fig. 4b. Such a chaotic attractor A is generally the final effect of a period-doubling route, set off by the appearance of a stable cycle on the closed invariant curve Γ. The behaviour of the trajectory in such a case is a kind of "permanent" erratic transient. The phase point wanders inside a chaotic area in an unpredictable way. However, as we shall show in Section 5, in the noninvertible case the structure of the phase-plane in zones with a different number of rank-1 preimages (also called Riemann foliation[9] in [20]), enables us to predict the strip inside which the state variables are confined. That is, even if, given a state, we cannot predict what will be the state in the next period, we can determine its lower and upper bound.

INSERT FIG. 4 APPROXIMATELY HERE

[9] As it is described in [20], in the case of two-dimensional noninvertible maps the phase-plane can be identi¯ed with several \sheets", each one being associated with one inverse of the map. The noninvertibility is thus characterized by the overlapping of di®erent sheets constituting the regions Z_j (with j di®erent rank-1 preimages) and the boundaries of these regions are generally given by the critical curves of rank ¡ 1, crossing which the number of distinct rank-1 preimages changes. This characterization is known as the foliation of the Riemann phase-plane.

As c increases, several regimes with "periodic windows" and "chaotic areas" may be observed. This regime is a two-dimensional analogue of what occurs in one-dimensional chaotic maps. We may think for example of the well known logistic map $x^{0} = f(x)$, $f(x) = {}^{1}x(1 ¡ x)$, and remember the complex mechanism giving the intervals of values of the parameter ^{1} in which there exists an attracting cycle as well as the intervals with chaotic dynamics. See the "box-within-a-box" mechanism described in [16] and similar two-dimensional behaviour described in [20]. It is well known that, on increasing the parameter ^{1} in the logistic map, the appearance of the attracting cycle of period three comes from a "previous" chaotic regime, and that the attracting 3-cycle is surrounded by a chaotic repellor, a kind of "invisible chaos" given by a set with the same characteristics of the set Λ previously described. Returning to our two-dimensional model, on increasing c (at values of the parameter a not too high), we can observe the appearance of a similar periodic regime, which persists as c approaches the value 1. An example of an attracting cycle appearing after the chaotic regime is given in Fig. 4c. We note that in this case a strange repellor Λ surrounding the stable cycle is likely to exist, and it is possible that looking at the trajectories in the "short period" there is not much difference between the case of Fig. 4b and that of Fig. 4c. The difference is evident in the long period or when the initial state is quite close to a periodic point of the cycle. In all the three situations shown in Fig. 4 we may consider the existing attractor (a closed curve Γ, a chaotic area A or a stable cycle) as "robust" with respect to external influences. In fact, the basin B(1) is quite far from such attracting sets and almost all the points in the region of the phase-plane shown in the figures have a similar qualitative behaviour. This kind of "robustness" is increased at lower values of a. When crossing the Hopf-curve at low values of a, an attracting closed curve Γ is observed but no route to chaotic regimes: we have numerically observed that the oscillatory behaviour persists and the oscillations become wider as a is decreased. Whereas, on increasing a the system goes towards a less stable regime, as already remarked in the previous section. For example, at $a = 1$ we have already seen the stable fixed point coexisting with an attracting 4-cycle in Fig. 2c. On increasing c from that situation we cross the Hopf-curve and an attracting closed invariant curve Γ appears. However we already know from Fig. 2c that O is not far from the boundary of its basin, and the same is true for Γ, as shown in Fig. 5a. This leads us to foresee that the interval of values of c for which an attracting closed invariant curve exists

will be very short. In fact, a global bifurcation occurs when the attracting set has a contact with the frontier of its basin of attraction. In our example this contact occurs in a point belonging to the frontier between the basin of Γ and the basin of the 4-cycle A_4, $\mathcal{B}(\Gamma) \setminus \mathcal{B}(A_4)$. Thus, after the contact, the only surviving attractor is the 4-cycle A_4, as shown in Fig. 5b. We note that this contact bifurcation also corresponds to a global bifurcation of the basin $B(A_4)$, which increases abruptly. The closure of $B(A_4)$ is now the white region in Fig. 5b and this new attracting set is also stable with respect to perturbations, being quite far from the boundary of its basin. We also note that only a few unstable cycles exist in that white region. From this cycle of period 4 the usual route to chaos via period doubling bifurcations is observed as c is further increased. A 4-piece chaotic attractor is shown in Fig. 5c and a global bifurcation leads to the reunion of the chaotic pieces into a single attractor of annular shape, shown in Fig. 5d.

INSERT FIG. 5 APPROXIMATELY HERE

Similarly, when we start from the situation shown in Fig. 2e and increase c we observe, on crossing the Hopf-curve, an attracting closed invariant curve Γ. Also now we shall have a global bifurcation causing the destruction of Γ but differently from the previous case: it cannot be predicted by the position of Γ with respect to $\mathcal{B}(1)$. In fact, as shown in Fig. 6a, Γ is quite far from that boundary. But it is the existence of the strange repellor Λ that will cause the global bifurcation. A contact between Γ and the strange repellor causes a homoclinic explosion (or Γ-explosion) which transforms the strange repellor into a strange attractor, as shown in Fig. 6b, after a very small increase of c. Such a global bifurcation has a very strong effect on the "observed attractor" because after the disappearance of the attracting set around O the generic trajectory wanders, aperiodically, within the chaotic set (which was previously "invisible", except for the transient part of a trajectory).

INSERT FIG. 6 APPROXIMATELY HERE

4.3 Crossing the Flip-curve

From the examples seen up to now, it is clear that the increase of the parameter a causes an increase of the dimension of the basin $B(1)$, i.e. of the

points having a divergent trajectory. Thus, from a practical point of view, this is a regime which must be controlled and possibly avoided.

In any case let us increase a so that the parameters approach the Flip-curve, and correspondingly the attractor has a lower basin of influence. This situation may also occur at the extreme conditions, as shown in Fig. 7a, where the attracting fixed point O may be considered as "practically unstable" by virtue of the fact that its basin is so narrow, and surrounded by points with divergent trajectories. It is clear that an increase of the value a, causing the flip bifurcation of O, shall give rise to a stable 2-cycle. And we may think that the usual flip-cascade shall occur. Whereas, after a few (say k) flip bifurcations the cycles of period 2^k created approach the basin boundary (see Fig. 7b). Then, a contact bifurcation (like that occurring to Γ in the previous example) causes the disappearance of the attractor, after which the generic trajectory in the phase plane is divergent. Note that also a decrease in the parameter c, when a has quite high values, causes a similar dynamic behaviour. For example, starting from the case shown in Fig. 3a a decrease of the parameter c causes the crossing of the Flip-curve. Similarly to the previous example we observe an attracting 2-cycle, followed by an attracting 4-cycle, and then the disappearance of the attractor.

INSERT FIG. 7 APPROXIMATELY HERE

5 Role of the critical curves in the global bifurcations

The goal of this section is to enter in more detail into the mechanism of some of the global bifurcations. We shall do this by following the examples already considered in Section 4, showing how the noninvertibility of the map (which at first sight seems to lead to an increase of difficulty) allows us to easily explain several phenomena. We use the powerful technical tool given by the critical curves, which have been determined, for our map, in Section 3.3. We first use the critical curves to construct an absorbing area, i.e. an area bounded by a few arcs of critical curves LC, LC_1, ..., which attracts nearby points and is trapping (once inside, a trajectory can never escape). Clearly, inside one absorbing area we have at least one attracting set. As we

shall see, inside an absorbing area several attractors may follow one another, and the area itself may undergo global bifurcations.

The reader who knows the role of the critical points (local extrema) in the dynamics of one-dimensional noninvertible maps (see kneading theory in [11] and [10]) can easily appreciate how the critical curves represent the corresponding two-dimensional analogue. Just as it occurs for the local extrema in one-dimensional maps, the critical curves bound the foliation of the Riemann phase plane. We shall use the notation introduced in [20], to which we refer the reader for further details and examples. One of the main applications of the critical curves and of the absorbing areas consists in a quick and easy method to determine whether a repelling node or focus is a snap-back-repellor, as described below. But let us start an analysis of some simple qualitative behaviour.

5.1 Absorbing areas

We consider again the case shown in Fig. 4a. As the parameter c is increased the closed invariant curve Γ increases in size, and the noninvertibility of T comes to play a role as Γ approaches the critical curve LC_{-1} and then crosses it. Note that from Fig. 4a it seems that Γ is closer to LC than to LC_{-1} and one might think that a contact with LC will come first. But this is impossible given the structure of the Riemann foliation of the zones Z_1-Z_3 bounded by LC. To make a one-dimensional analogue, think at an interval J mapped by the logistic map $f(x) = {}^{1}x(1 - x)$. It is clear that $f(J)$ cannot cross the local maximum, denoted by C; $f(J)$ can only have C on the boundary and this can occur only if J includes the critical point C_{-1}. In the same way the critical curve LC cannot be crossed, the arcs crossing LC_{-1} are mapped by T into arcs "folded" on LC and tangent to that curve. Consider Fig. 8a. The crossing of LC_{-1} causes the appearance of "oscillations" in the smooth shape of Γ, due to the "folding" on LC and its further images. In fact, the portion of Γ which crosses LC_{-1} (in the points a_0 and b_0) is folded back with two points of tangency on LC (see a_1 and b_1 in Fig. 8a, where also the points a_2 and $b_2$of tangency on LC_1 are indicated as well as the points of tangency on critical curves of higher rank). More crossings of LC_{-1} as c increases may occur, which are the cause of more oscillations in the shape of Γ, as shown in Fig. 8b. We remark that such qualitative changes in the shape of Γ modify the quasiperiodic orbit of the asymptotic trajectories. Moreover, we

can completely define the area enclosing Γ by means of the critical curves. In fact, making use of the properties decsribed in Chapter 4 of [20], we select a suitable piece of LC_{i1}, and with a few iterates of this segment we get a closed area, simply connected, which is mapped into itself by T (see again Figs. 8a,b); Γ is tangent to the boundary of this area in several points (those on LC and their images). Moreover, with some more iterates of the same arc on LC_{i1}, an "inner" boundary is also obtained, so that an absorbing area of annular shape is defined (Fig. 8b). Γ is tangent both to the external and internal boundaries of that area (see the enlargement of Fig. 8c).

INSERT FIG. 8 APPROXIMATELY HERE

As c is further increased, several attracting sets alternate inside the absorbing area: quasi-periodic orbits, periodic orbits, flip sequences leading to chaotic dynamics, as it was shown in Fig. 4 in the previous section. The annular attracting set of Fig. 4b is inside an annular absorbing area. Another example is given in Fig. 9a. A small portion of LC_{i1} in that figure was iterated 19 times and the resulting set is an invariant absorbing area A_1, inside which the trajectories are confined. A trajectory is shown in Fig. 9b. What is remarkable in the use of the critical curves is that these allow us to predict the lower and upper bounds of both the state variables. Such limiting values can be obtained from the rectangle bounding the absorbing area.

Looking at the iterated points of a trajectory we shall see that a global bifurcation occurs at a particular value of c, say c^{α} (in our example $0{:}525 < c^{\alpha} < 0{:}526$). Before, for $c < c^{\alpha}$, we have iterated sequences all inside the annular absorbing area as in Figs. 9a,b, while immediately after, for $c > c^{\alpha}$, we shall have iterated points which also go outside, although such "bursts" are quite rare, as shown in Fig. 9d. This is the effect of a global bifurcation due to the contact of the critical curves on the boundary of the absorbing area A_1 with a chaotic repellor existing outside. Such a contact destroys the invariance property of the area A_1 and after the bifurcation the iterated points can escape the old area A_1.

This bifurcation can be detected also by use of the critical curves. In fact, for $c < c^{\alpha}$ the iterations of the small segment a_0b_0 of LC_{i1} define an area A_1 which is invariant, so that all the iterates $T^n(a_0b_0)$, $n > 0$, belong to that area. While for $c > c^{\alpha}$ the area obtained by iterating the segment a_0b_0 of

LC_{i1} is no longer invariant, i.e. there exists a positive integer m such that $T^m(a_0b_0)$ has points also outside. This corresponds to an "explosion" of the attracting set. After the contact the new iterates will cover a wider area; but which one? Again we can predict the area by looking at the images of the critical segments. A wider portion of LC_{i1}, see a_0c_0 in Fig. 9c, is such that with a finite number of iterates we obtain a new wider absorbing area A_2 (which includes the old area A_1, no longer invariant). The boundary of the new absorbing area is strictly included in $[\bigcup_{n=1}^{12} T^n(a_0c_0)$. From Fig. 9d it is evident that A_2 is the smallest invariant absorbing area existing after the contact bifurcation that destroys A_1.

INSERT FIG. 9 APPROXIMATELY HERE

This global bifurcation is very similar to the one we have already observed in Section 4, causing the "Γ-explosion". That is, a drastic change of the structural shape of the attractor, from a closed invariant curve Γ (Fig. 6a) to the chaotic area in Fig. 6b. Note that also before such a contact bifurcation we could predict the effect of the bifurcation by use of the critical curves. Fig. 10 represents the same closed invariant curve Γ of Fig. 6a, but inside an invariant area A bounded by a few arcs of critical curves, obtained by taking the images of the small segment a_0c_0 on LC_{i1}. Clearly, in Fig. 10, such an invariant area also includes the chaotic repellor that we know exists outside Γ, and its shape perfectly reproduces the attractor shown in Fig. 6b, existing soon after the contact. While before the contact all the trajectories starting inside A, except for a set of zero Lebesgue measure, converge to Γ, after such a bifurcation the generic trajectory is spread out, wandering among the repelling cycles existing outside, as shown in Fig. 6b. But such iterations cannot escape the invariant area A (Fig. 10), so that the iterated points are forever confined inside it. Note that in this case we could determine an upper and lower bound of the state variables, also before the contact bifurcation, predicting the effect of a global bifurcation. This is quite important if we want to take account of "shocks" that change the values of the parameters of the model.

INSERT FIG. 10 APPROXIMATELY HERE

It is now clear that also the sequences of bifurcations shown in Fig. 5 of the previous section all occur inside a similar absorbing area. Regular and

chaotic dynamics alternate inside the annular area around the repelling fixed point O.

5.2 How to detect the homoclinic bifurcation of a snap-back repellor

Let us return to the annular absorbing area A_2 shown in Fig. 9. We see that a hole W exists including the fixed point O, a repelling focus. As locally the trajectories spiral out of O, it turns out that all the points of W n fOg have trajectories entering the trapping annular absorbing area. Thus, in such a situation, although the fixed point O is repelling, we cannot find any homoclinic orbit of the origin. The existence of a homoclinic orbit of a repelling focus O often causes the appearance of a set which "attracts" and then "repells" (as occurs in the case of homoclinic orbits to saddles). A trajectory behaves chaotically far from O, but then it approaches O and seems attracted, but soon after it is repelled away. This occurs with intermittence, and with unpredictable return time near O. The existence of such homoclinic orbits is a powerful tool used to prove the true chaotic nature of the observed trajectories. In fact, Marotto [19] first proved that such an orbit for a repelling node or focus implies the existence of chaos in the sense of Li and Yorke (see [17]).

In our example, the fixed point O is a repelling focus for a wide interval of values of c, i.e. for c > c̄ ' 0:48. However when is it possible to find some homoclinic orbits of O? Certainly we cannot look for homoclinic orbits as long as the map has a unique inverse, because in invertible maps, homoclinic orbits of repelling nodes and foci cannot exist: but in our example, where a = 0:8, the map T is noninvertible in all the range of c for which O is unstable. In the regime of non-invertibility of T we can make use of the properties of the critical curves of the map. In fact, as proved in [13], the critical curves provide a powerful technique that helps us in finding the homoclinic orbits of cycles. For example, although chaotic dynamics certainly exist for the map in the cases shown in Fig. 9, we can state that these do not involve the fixed point O. In fact, as long as the repelling fixed point belongs to an absorbing area, bounded by critical curves, as shown in that figure, but with a hole W surrounding O, then we can prove that all the preimages of any rank of O (which are infinitely many) are outside the absorbing area (and thus outside the chaotic area there shown). This is true for all the points

belonging to the hole W defined by the annular absorbing area, and it is an immediate consequence of the fact that the absorbing area is trapping. We note that other qualitative changes occur in the absorbing area, with tongues approaching O, but as long as the rank-1 preimages of O distinct from itself are outside the invariant absorbing area, then the critical curves leave an empty hole around O (see Fig. 11a and the enlargement in Fig. 11b), and no homoclinic points of O can exist. This is because for any $n > 0$, $T^{-n}(O)$ can never return near O.

Then we can easily conclude that as c increases, the first homoclinic bifurcation, or homoclinic explosion, necessarily occurs when one of the rank-1 preimages of the fixed point O, from the outside of the absorbing area A_2, falls on the boundary and crosses it, through an LC arc. This occurs approximately at $c \simeq 0.5335$. Even if we would not compute the rank-1 preimages of O, we could be sure that we are at the homoclinic bifurcation of the fixed point because at this particular value the images of the critical curves of LC must cross through O and, as shown in the enlargement of Fig. 11d, we can see that all the images LC_{12}, LC_{13}, LC_{14}, ... (LC_k for $k \geq 12$) of the LC curve cross the fixed point O, which means that one of its rank-1 preimages, say O_{-1}, lies now on the boundary of the absorbing area, on the curve LC_{11}.

At this bifurcation value homoclinic orbits of O (and infinitely many) appear. In fact, the point O_{-1} on the curve LC_{11} of the boundary of the absorbing area must have a rank-1 preimage on the curve LC_{10}, and so on iteratively, up to a preimage in the segment of LC_{-1} inside the area A. In its turn this point has an arborescent sequence of preimages of any rank inside the absorbing area A, and infinitely many of these preimages can be obtained with the local inverse near the fixed point O, thus giving critical homoclinic orbits. In fact, when c is at the first homoclinic bifurcation value, the characteristic property (see also [13]) is that all the homoclinic orbits of O are critical (i.e. include a critical point). While soon after the bifurcation value infinitely many non-critical homoclinic orbits of O exist.

In the same way as homoclinic orbits appear, these can also disappear (reverse bifurcation). In our example, such forward and backward bifurcations occur as the parameter c increases. Homoclinic orbits appear at about $c \simeq 0.5335$ and disappear at $c \simeq 0.562$. In fact, it is easy to see that O_{-1} crosses again the boundary of the absorbing area, now from inside to outside, thus destroying all the homoclinic trajectories. For $c > 0.562$, homoclinic orbits

of O no longer exist (see Figs. 11e,f).

INSERT FIG. 11 APPROXIMATELY HERE

This gives us the opportunity to generalize the same mechanism of homoclinic bifurcations to cycles. As we have seen in the previous example, in which the parameter a is fixed (a = 0:8) and we increase c from the value c̄, on the Hopf-curve, towards 1, homoclinic orbits of the fixed point O exist for a very narrow interval of c-values. However we have seen trajectories which seem chaotic for several other intervals of values of c. How can we prove that these regime are truly chaotic? It is a simple matter to note that the same reasoning performed on the fixed point can hold for any cycle. Inside the absorbing area there are infinitely many unstable cycles repelling nodes or foci. Consider one of them, say of period k. Then the periodic points are fixed points for the map T^k and for them we can look for the existence of homoclinic orbits. As above, we have simply to consider the preimages of these periodic points. Whenever one of these preimages is inside the invariant area, then homoclinic orbits of the cycle exist. Also: when the images of the small arcs of LC_{i1} (which give the "germ" to construct the boundary of the absorbing area) cross through a repelling periodic point of the k-cycle (as it was shown in Fig. 11d), we are at the snap-back-repellor bifurcation of that cycle.

We remark that the existence of homoclinic orbits is a sure indication of chaotic dynamics, but often of what is also called "invisible chaos". For example, chaos also occurs in the case shown in Fig. 4c, where the generic numerically observed trajectory is convergent to a cycle of period-4. Let us recall here a one dimensional analogue to better clarify the issue, considering the box-within-a-box bifurcation structure occurring in the logistic map $f(x) = {}^1x(1 - x)$. One of the widest intervals with periodic orbit is the one associated with a cycle of period 3: for an interval of ¹-values we have an attracting 3-cycle which attracts almost all the trajectories in the interval $[0; 1]$. However we are in a "chaotic regime" because an invariant set Λ on which the restriction of the map is chaotic (in the purest sense) exists (and this is true for any value of ¹ after the Feigenbaum point).

Similarly, also in the two-dimensional case, whenever a homoclinic orbit of some cycle exists (as it is certainly the case for many repelling cycles in Fig. 4c), we can say that an invariant set Λ exists on which the map is chaotic,

but "how big" is the set Λ is not known. Generally such sets are of zero Lebesgue measure. When they are "embedded" in some bounded absorbing area, then we can argue their presence through the "chaotic transients" before the trajectory settles down on some attracting cycle, as it was shown in Fig. 6a. Also chaotic dynamics such as those shown in Fig. 6b inside the absorbing area are generally chaotic transients of trajectories which ultimately may converge to a cycle of period so high that we cannot detect it by numerical simulations.

Consider the case shown in Fig. 11c: we can never observe the "end" of the numerically computed trajectory, which wanders around for a long time and then approaches the snap-back-repeller O, and is repelled out, again returns near O after a while and again it is pushed back, and so on. Fig. 11c clearly shows the many points lying near O, and also we can observe a sort of "structure" inside this small portion of the phase-plane. This is due to the foliations of the Riemann plane; the points of a trajectory visit more frequently the critical curves, and the "structure" which is evident in Fig. 11c is due to arcs of critical curves LC_k, $k > 1$.

6 A simple stochastic extension

The aim of the present section is to present numerical examples showing how the critical-lines tools can help to understand the dynamic behaviour of the system in simple stochastic situations.

The introduction of stochastic factors into the model can be done in different ways. For our purposes, we simply suppose that the speed of adjustment of chartists' expectation c, instead of being fixed, is a random variable uniformly distributed between c_{min} and c_{max}. In doing so we capture, albeit in a crude way, the notion that the chartists adjust c up and down around some mean value, in response to randomly arriving market news. Such news rendering the chartists either aggressive (increase in c) or cautious (decrease in c) in their use of the trading rule. Under this assumption the stochastic trajectory is given by:

$$X_{t+1} = T_{c_t}(X_t) \ ,$$

where c_t is a random parameter uniformly distributed on the interval $[c_{min}; c_{max}]$ and T_{c_t} is the map given in (7) with parameter value c_t. Let us fix $a = 1{:}25$ and consider a regime in which the system has as its only attractor the stable

equilibrium O, with a wide and connected basin of attraction; for example let us assume c is uniformly distributed on the interval [0:59 ¨ 0:04]. The observed dynamic effect is that also the stochastic trajectory converges to the stable fixed point O, but its representation in the phase-plane is similar to a "cloud" around O (Fig. 12a).

The existence of an absorbing area A (inside which the transient and asymptotic dynamics are constrained to move) sufficiently far from the boundary of its basin @B(A) guarantees the "stability" of the "stochastic" model so obtained. In fact, the introduction of such a noise has in general the dynamic effect of changing the attractor of the deterministic model into a "cloud" having similar shape and the knowledge of the critical curves of the map (7) allows us to predict whether the new "stochastic" dynamics will be bounded inside a deterministic region or not. As an example let us fix a = 0:8 and consider an interval of values of c for which the deterministic model has an attracting set (a closed invariant curve, a chaotic attractor or a cycle) belonging to an absorbing area, say c uniformly distributed on the interval [0:52 ¨ 0:03]. Figs. 12b and 12c show the attractors and the absorbing areas of the limiting cases c = 0:49 and c = 0:55, respectively. Assuming an initial condition near the repelling fixed point, we see (Fig. 12d) that the stochastic trajectory consists in points belonging to a bounded area (although its contour is not well determined). The width of this region obviously depends on the range assumed for c, which also determines the nature of the underlying deterministic attractors

INSERT FIG. 12 APPROXIMATELY HERE

It is difficult to draw conclusions about the stochastic behaviour of the model starting from a deterministic framework. It would be interesting to try to prove the existence of a deterministic area, say S, which is trapping for the stochastic model at least for a number of iterations sufficiently high to be considered of interest in an applied context. A first step in this direction could be the analysis of the dynamic behaviour of the limiting cases $T_{c_{min}}$ and $T_{c_{max}}$, as we have done in the previous example, also in order to predict whether we are in a stable regime of the stochastic model or not. In fact it is clear that when values of a and c are involved for which the basin B(1) of the deterministic map T_c approaches the attracting sets then we can say that the stochastic approach is highly unstable. Consider as an example the

situation represented in Fig. 13, where we assume c_t uniformly distributed on the interval [0:595 ¨ 0:045]. The deterministic limiting maps $T_{0:55}$ and $T_{0:64}$ have as attracting sets the fixed point O, on which the trajectory settles down after a chaotic transient, and a 4-piece chaotic attractor, respectively. These attractors are represented, together with the basin B(1), in Figs. 13a and 13b. We note in particular that the basin of the attractor in Fig. 13b is multi-connected with infinitely many holes. The stochastic map T_{c_t}, c 2 [0:595 ¨ 0:045], starting from the same initial condition used for the limiting maps, gives rise to a trajectory which is divergent, after a chaotic transient, as shown in Fig. 13c.

INSERT FIG. 13 APPROXIMATELY HERE

7 Conclusions

In this paper we have developed a discrete time model of asset price dynamics, based on the interaction of two types of traders: rational fundamentalists, who form rational expectations on the fundamental value of the asset and whose demand is an increasing function of the difference between the fundamental value and the current price, and chartists, a group basing its trading decisions on an analysis of past price trends, whose demand is an S-shaped function of the expected return differential with an alternative asset. To clarify the adjustment process of the share price in the market, we assume the existence of a market maker, whose role is to set excess demand to zero at the end of each trading period by taking an off-setting long or short position, and who announces the next period price as a function of the excess demand. We have highlighted the role of the two types of traders by showing the effect, on the local and global dynamics, of the key parameters, namely the "strength" of fundamentalist and chartist demand (a and ®, respectively), and the speed of adjustment of chartists' expectations (c). In particular we have clarified how the strength of chartist demand ® affects the local stability of the equilibrium, by showing that for sufficiently low values of ® the equilibrium is stable for a wide range of values of the fundamentalist parameter a and for any level of the chartists' reaction speed c ($0 < c \cdot 1$); while when ® is sufficiently high, i.e. chartist demand is relatively strong, the ability of fundamentalists' demand to stabilise the system is restricted to a

fairly narrow range of the parameter a. Our analysis has then focused on the global dynamical behaviour observed in this latter case. First we have shown that also when the equilibrium is locally stable other dynamic phenomena arise for sufficiently high values of c and a, such as chaotic transients before the convergence to the stable equilibrium or coexistence of attractors. We have then performed a detailed analysis of the dynamic phenomena occurring when, by increasing the parameter c, the equilibrium O becomes unstable via a Neimark-Hopf bifurcation: we have numerically observed that when this bifurcation occurs at sufficiently high values of the parameter a, an increase of c leads to oscillatory behaviour which may become chaotic around O, and as c approaches the value 1 the dominating state is an attracting cycle (although coexisting with a strange repellor) with a wide basin of attraction. In this global analysis, the theory of critical curves and various numerical tools have been extensively used.

We have paid particular attention to the analysis of the homoclinic bifurcation of fixed points and cycles, leading to a chaotic regime. The existence of chaotic behaviour in a model of asset price dynamics similar to ours has been detected in [12]. But the present paper follows a different approach based on the theory of critical curves and is able to explain in detail the appearance of chaotic dynamics.

Finally, we have suggested an extention of the model beyond its deterministic nature, showing how the analysis of deterministic dynamics via the critical-lines tools can help to understand the dynamic behaviours of the system in simple stochastic situations.

Future developments of the model introduced here would be to analyse the dynamics of the three dimensional map which arises when the dynamics of the market for the alternative asset is also taken into account (as discussed briefly in section 3). It is also important to focus on attemps of each group to learn about their economic environment in the face of stochastic factors (capturing for example the random arrival of new events in the market). Some initial attempts in this directions are outlined in [1] and [7]

Finally, in order to focus on the dynamics induced by the interaction of fundamentalists and the speculative behaviour within a two-dimensional map, we have left in the background the dynamics of the wealth of the two groups. This is perhaps justifiable in the present context since an exponential utility of wealth function underlies both the fundamentalist and chartist demand function. As is well known demand functions in this case are inde-

pendent of wealth. Clearly in the long term the evolution of the wealth of each group will also determine their economic behaviour, and such evolution needs to be modelled. Chiarella and He [9] have developed a model of heterogeneous agents with logarithmic utility function which takes explicit account of the wealth dynamics of each group, but the analysis of this model is only possible via computer simulations. However the insights into the dynamics of speculative behaviour gained via the simpler model of this paper are useful in attempting to understand the dynamics of the more complete models of Chiarella and He [9] as well as those of Chen and Yeh [4].

Acknowledgments. This work has been performed with the financial support of CNR, Italy, and within the scope of the national research project "Nonlinear Dynamics and Stochastic Models in Economics and Finance", MURST, Italy. Financial support of the Australian Research Council is also acknowledged. We would like to thank the two anonymous referees for helpful comments and suggestions. We also thank Gian Italo Bischi for having read a previous version of this paper and pointing out some misconceptions. The usual caveat applies.

Appendix: Derivation of asset demand functions

We use the subscript $i \in \{f, c\}$ to denote fundamentalists or chartists.

Let $\Omega_{i;t}$ be the wealth of agent i and $Z_{i;t}$ be the fraction of this wealth that agent i decides to invest in the risky asset, at time t. The agent's wealth at time $(t+1)$ will then be given by:

$$\Omega_{i;t+1} = \Omega_{i;t} + \Omega_{i;t}(1 - Z_{i;t})g_t + \Omega_{i;t}Z_{i;t}(P_{t+1} - P_t) \ ,$$

where g_t is the return on the alternative asset. Agent i computes the conditional mean and variance of $\Omega_{i;t+1}$(denoted by $E_{i;t}[\Omega_{i;t+1}]$ and $V_{i;t}[\Omega_{i;t+1}]$, respectively) assuming that $(P_{t+1} - P_t)$ is conditionally normal, thus:

$$E_{i;t}[\Omega_{i;t+1}] = \Omega_{i;t} + \Omega_{i;t}(1 - Z_{i;t})g_t + \Omega_{i;t}Z_{i;t}E_{i;t}[P_{t+1} - P_t] \ ,$$

$$V_{i;t}[\Omega_{i;t+1}] = Z_{i;t}^2\Omega_{i;t}^2 V_{i;t}[P_{t+1} - P_t] \ .$$

Assuming that each group of agents has an exponential utility of wealth function, each agent seeks $Z_{i;t}$ so as to maximise

$$E_{i;t}[-\exp(-\alpha_i \Omega_{i;t+1})] \ ,$$

where $\mathbb{R}_i$ is agent i's risk aversion coefficient. Under the assumption that $\Omega_{i;t+1}$ is conditionally normally distributed, this problem is equivalent to

$$\max_{z_{i;t}} \left[E_{i;t}[\Omega_{i;t+1}] - \frac{\mathbb{R}_i}{2} V_{i;t}[\Omega_{i;t+1}] \right] .$$

The solution to this optimization problem is:

$$\mathbb{3}_{i;t} \cdot z_{i;t}\Omega_{i;t} = \frac{E_{i;t}[P_{t+1} - P_t] - g_t}{\mathbb{R}_i V_{i;t}[P_{t+1} - P_t]} .$$

We note that $\mathbb{3}_{i;t}$ is the demand by agent i for the risky asset.

The two groups of agents essentially differ in the way they calculate the mean and variance of the price change over successive time intervals.

Fundamentalists, with their assumed superior knowledge of market fundamentals, believe that the asset price follows a mean reversion process with the fundamental value being the long run mean. Hence they calculate that the expected excess return is proportional to the difference between the current asset price and the fundamental value, i.e.:

$$E_{f;t}[P_{t+1} - P_t] - g_t = \mathbb{'}(W_t - P_t) ,$$

where $\mathbb{'}$ is the speed of mean reversion estimated by the fundamentalists. They also assume that the conditional variance of price changes is constant, i.e.:

$$V_{f;t}[P_{t+1} - P_t] = v_f .$$

Thus the fundamentalist asset demand becomes:

$$\mathbb{3}_{f;t} = \frac{\mathbb{'}(W_t - P_t)}{\mathbb{R}_f v_f} ,$$

which becomes (1) when we identify the strength of fundamentalist demand a with $\mathbb{'} = (\mathbb{R}_f v_f)$.

Chartists, on the other hand, calculate $E_{c;t}[P_{t+1} - P_t]$ by extrapolating past prices changes according to (3). Thus:

$$\mathbb{3}_{c;t} = \frac{\tilde{A}_{t;t+1} - g_t}{\mathbb{R}_c v_c} .$$

Unlike the fundamentalists, the chartists change their estimate v_c of the conditional variance according to the magnitude of $|\tilde{A}_{t;t+1} - g_t|$. As this quantity

becomes larger they expect greater volatility and increase their estimate v_c, hence lowering the slope of their demand function. It is this behaviour that explains the levelling off of the slope of chartist demand as $|\tilde{A}_{t;t+1} - g_t|$ becomes larger, and hence we derive the chartist demand function (2).

References

[1] A. Agliari, C. Chiarella and L. Gardini, The feedback between asset prices and learning in a simple model of heterogeneous agents, Working Paper, School of Finance and Economics, University of Technology, Sydney, 1999.

[2] A. Beja and M.B. Goldman, On the dynamic behavior of prices in disequilibrium, Journal of Finance, 35, 1980, 235-248.

[3] W. Brock and C. Hommes, Heterogeneous beliefs and routes to chaos in a simple asset pricing model, Journal of Economic Dynamics and Control, 22, 1998, 1235-1274.

[4] S.H. Chen and C.H.Yeh, Modelling speculators with genetic programming, in P. Angeline et al. (eds.), Evolutionary Programming VI, Lecture Notes in Computer Science, vol. 1213, Springer-Verlag, 1997, 137-147.

[5] C. Chiarella, The dynamics of speculative behaviour, Annals of Operations Research, 37, 1992, 101-123.

[6] C. Chiarella, R. Dieci and L. Gardini, Asset price dynamics in a financial market with fundamentalists and chartists, submitted to Discrete Dynamics in Nature and Society, 2000.

[7] C. Chiarella and X. He, Heterogeneous beliefs, risk and learning in a simple asset pricing model, Working Paper n. 18, Quantitative Finance Research Group, School of Finance and Economics, University of Technology, Sydney, 1999, also forthcoming in Computational Economics.

[8] C. Chiarella, R. Dieci and L. Gardini, A dynamic analysis of speculation across two markets, Working Paper, School of Finance and Economics, University of Technology, Sidney, 2000.

[9] C. Chiarella and X. He, Wealth Dynamics, Heterogeneous Beliefs and Learning, Working Paper, Quantitative Finance Research Group, School of Finance and Economics, University of Technology, Sydney, 2000.

[10] P. Collet and J.-P. Eckmann, Iterated maps on the interval as dynamical systems, Birkhauser, Basel-Boston, 1980.

[11] R.L. Devaney, An Introduction to Chaotic Dynamical systems, The Benjamin/Cummings Publishing Co., Menlo Park, California, 1987.

[12] F. Fernandez-Rodriguez and M.D. Garcia-Artiles, A model of speculative behaviour with a strange attractor, Working Paper, Departimento de Métodos Cuantitativos para la Economía y Gestión, Universidad de Las Palmas de Gran Canaria, 1998.

[13] L. Gardini, Homoclinic bifurcations in n-dimensional endomorphisms due to expanding periodic points, Nonlinear Analysis, T.M.&A., 23, 1994, 1039-1089.

[14] M.B. Goldman and A. Beja, Market prices vs. equilibrium prices: returns' variance, serial correlation, and the role of the specialist, Journal of Finance, Vol. 34, n. 3, 595-607, 1979.

[15] I. Gumowski and C. Mira, Dynamique Chaotique, Cepadues Ed., Toulouse, 1980.

[16] C. Mira, Chaotic Dynamics, World Scientific, Singapore, 1987.

[17] T.Y. Li and J.A. Yorke, Period three implies chaos, American Mathematical Monthly, 82, 1975, 985-992.

[18] T. Lux, The socio-economic dynamics of speculative markets: interacting agents, chaos and the fat tails of return distributions, Journal of Economic Behaviour and Organization, 33, 1998, 143-165.

[19] F.R. Marotto, Snap-back repellers imply chaos in R^n, Journal of Mathematical Analysis and Applications, 72, 1978, 199-223.

[20] C. Mira, L. Gardini, A. Barugola and J.C. Cathala, Chaotic Dynamics in Two-Dimensional Noninvertible Maps, World Scientific, Singapore, 1996.

[21] T. Puu, Attractors, Bifurcations and Chaos, Springer, N.Y., 2000.

[22] E.C. Zeeman, On the unstable behaviour of stock exchanges, Journal of Mathematical Economics, 1, 1974, 39-49.

FIGURE CAPTIONS

Fig. 1. The dark grey regions in Figs. 1a and 1b show the domain of stability of the equilibrium point O in the plane of the parameters c (speed of adjustment of chartists' expectations) and a (strength of fundamentalists' demand). The light grey regions represent the domain of noninvertibility of the map T in the same $(c; a)$ parameter plane. Fig. 1a is obtained with values of the parameters $\bar{p}$, ®, g such that $\bar{p}k'(0) = \bar{p}®=(1+g^2) \cdot 1$: in this case the domain of stability includes any value $c \in (0;1)$ for sufficiently low values of a (i.e. for $a < 2=\bar{p}$), and the stability can be lost only via a Flip bifurcation as a is increased. Fig. 1b describes the opposite case, $\bar{p}k'(0) > 1$, where stability can be lost also via a Neimark-Hopf bifurcation at low values of a. Fig. 1 also shows that for sufficiently low values of a (i.e. for $a < 1=\bar{p}$) the map is invertible for any value $c \in (0;1)$. In the case of Fig. 1b the noninvertibility region is wider than in Fig. 1a.

Fig. 2. Different dynamic phenomena observed for values of the parameters for which the equilibrium point O is stable. Figs. 2a, 2c and 2e represent the dynamics in the phase-plane $(\tilde{A}; p)$, while Figs. 2b, 2d and 2f show, for each case (and the initial values indicated), the state variable p as a function of time. In the case of Figs. 2a and 2b the equilibrium point O is an attracting focus with a wide basin of attraction. In Fig. 2c the stable equilibrium point (whose basin is the white region) coexists with a 4-cycle (whose basin is the non-connected light grey region): Fig. 2d shows the trajectories of two nearby initial conditions (but in different basins), one giving damped oscillations towards O, the other converging to the 4-cycle. In Fig. 2e the stable fixed point coexists with a strange repellor, whose effect on the transient part of the trajectory is shown in Fig. 2f.

Fig. 3. For $\bar{p} = 2{:}6$, $g = 1$, $® = 2{:}5$, $a = 1{:}5$, $c = 0{:}48$ the fixed point O is the only attractor, but it may be considered as "practically unstable" due to the structure of its basin of attraction, which is very small and multi-connected (Fig. 3a). Two nearby initial conditions, even very close to O, may lead to very different dynamic behaviour: starting from the point $(0; -1{:}25)$ in the phase-plane we observe convergence to the equilibrium, while starting from the point $(0; -1)$ we observe divergence (Fig. 3b).

Fig. 4. Dynamic behaviour observed for $\bar{p} = 2{:}6$, $g = 1$, $® = 2{:}5$, $a = 0{:}8$ and by increasing c starting from outside the stability region of O, on the right of the Neimark-Hopf bifurcation curve in Fig. 1b: an attracting closed invariant curve (Fig. 4a), a chaotic attractor of "annular shape" (Fig. 4b), an attracting 4-cycle appearing after the chaotic regime (Fig. 4c).

Fig. 5. With a value of c slightly increased with respect to the situation represented in Fig. 2c, i.e. for $\bar{p} = 2{:}6$, $g = 1$, $® = 2{:}5$, $a = 1$, $c = 0{:}539$, we observe coexistence of a 4-cycle with a closed invariant curve Γ, created through a supercritical Hopf bifurcation (Fig. 5a). However Γ is very close to the boundary of its basin of attraction and, by increasing c further, the closed invariant curve disappears as soon as it has a contact with this boundary, leaving the 4-cycle as the only surviving attractor (whose basin is the white region in Fig. 5b). As c is further increased, we observe a 4-piece chaotic attractor (Fig. 5c), and the reunion of the chaotic pieces into a single attractor (Fig. 5d).

Fig. 6. For $\bar{p} = 2{:}6$, $g = 1$, $® = 2{:}5$, $a = 1{:}25$, as in Fig. 2e, but with a value of c slightly increased ($c = 0{:}594$), the only attractor is a closed invariant curve Γ which, differently from Fig. 5a, is now quite far from $@B(1)$ (Fig. 6a). As c is slightly increased from 0:594 to 0:595 (Fig. 6b) we observe the destruction of Γ due to the contact with a coexisting strange repellor: this contact causes the transformation of the strange repellor into a strange attractor (homoclinic explosion).

Fig. 7. For $\bar{p} = 2{:}6$, $g = 1$, $® = 2{:}5$, $a = 1{:}64$, $c = 0{:}52$ the only attractor is the equilibrium point O with a small (and multi-connected) basin of influence ((Fig. 7a). By increasing a so that the Flip-curve in Fig. 1b is crossed we observe a flip bifurcation that creates an attracting 2-cycle but the usual flip-cascade cannot occur because the basin boundary approaches the cycles of period 2^k (Fig. 7b, where we see the case $k = 3$).

Fig. 8. For $\bar{p} = 2{:}6$, $g = 1$, $® = 2{:}5$, $a = 0{:}8$, and by increasing c starting from outside the stability region of O, on the right of the Neimark-Hopf bifurcation curve in Fig. 1b, we observe a closed invariant curve Γ which increases in size. Since in this regime the map T is noninvertible, the crossing of LC_{i1} causes the appearance of "oscillations" in the shape of Γ, due to the "folding" on LC and its further images (Fig. 8a). More crossings are the cause of more oscillations (Fig. 8b). However an absorbing area of "annular" shape enclosing Γ can be completely defined by iterating a suitable piece of LC_{i1}. Γ is tangent both to the external and internal boundaries of

that area (see the enlargement of part of the absorbing area in Fig. 8c).

Fig. 9. An absorbing area of annular shape, defined by means of the critical curves (Fig. 9a), encloses the attracting set represented in Fig. 9b. The critical curves also allow us to detect the occurrence of global bifurcations, as the one caused by the contact of the boundary of the absorbing area with a strange repellor existing outside and leading to an explosion of the attracting set (Figs. 9c, 9d).

Fig. 10. In the situation already shown in Fig. 6a, i.e. for $\bar{}_p = 2{:}6$, $g = 1$, $® = 2{:}5$, $a = 1{:}25$, $c = 0{:}594$ the shape of the absorbing area enclosing the closed invariant curve Γ allows us to predict the drastic change in the structural shape of the attractor observed in Fig. 6 by slightly increasing the value of c.

Fig. 11. For $\bar{}_p = 2{:}6$, $g = 1$, $® = 2{:}5$, $a = 0{:}8$, $c = 0{:}5298$ we observe a chaotic attractor, enclosed into an annular absorbing area, bounded by critical curves. These critical curves leave an empty hole around the repelling fixed point O and correspondingly the preimages of any rank of O are outside the absorbing area (Figs. 11a, 11b). When, by increasing c, one of the rank-1 preimages of the fixed point O (say $O_{i\,1}$) falls on some critical curve on the boundary of the absorbing area and crosses it (at $c \;'\; 0{:}5335$), we observe the first homoclinic bifurcation of the repelling fixed point O, indicated also by the crossing through O of all the images of the critical curve (Fig. 11d). Soon after the bifurcation infinitely many homoclinic orbits of O exist, and the hole surrounding O disappears (Fig. 11c). On increasing further c a reverse bifurcation occurs (at $c \;'\; 0{:}562$), causing the disappearance of homoclinic orbits: $O_{i\,1}$ crosses again the boundary of the absorbing area, now from inside to outside (Fig. 11e), and a new hole appears around O (Fig. 11f).

Fig. 12. Numerical results obtained by introducing stochastic factors into the model. Assuming $\bar{}_p = 2{:}6$, $g = 1$, $® = 2{:}5$, $a = 1{:}25$, c stochastic and uniformly distributed on the interval $[0{:}55; 0{:}63]$ the resulting stochastic trajectory converges to the stable fixed point and its representation in the phase-plane is similar to a "cloud" around O (Fig. 12a). Fig. 12d shows a stochastic trajectory obtained for $\bar{}_p = 2{:}6$, $® = 2{:}5$, $g = 1$, $a = 0{:}8$ and under the assumption that c is uniformly distributed on the interval $[0{:}49; 0{:}55]$, while Figs. 12b and 12c show the attractors and the absorbing areas existing in the deterministic limiting cases $c = 0{:}49$ and $c = 0{:}55$, respectively.

Fig. 13. The knowledge of the structure of the basins of attraction in the deterministic case helps us to predict whether we are in a "stable"

regime for the stochastic model or not. Assuming $\bar{\ }_{\mathsf{p}} = 2{:}6$, $\mathsf{g} = 1$, $® = 2{:}5$, $\mathsf{a} = 1{:}25$ and c uniformly distributed on the interval $[0{:}55; 0{:}64]$, we obtain stochastic divergent trajectories, after a chaotic transient, as shown in Fig. 13c. Figs. 13a and 13b show the attractors existing in the deterministic limiting cases $\mathsf{c} = 0{:}49$ and $\mathsf{c} = 0{:}55$, respectively, together with their basins of attraction. We note in particular that the basin of the attractor shown in Fig. 13b is multi-connected with infinitely many "holes" of points with divergent trajectories.

Fig. 1

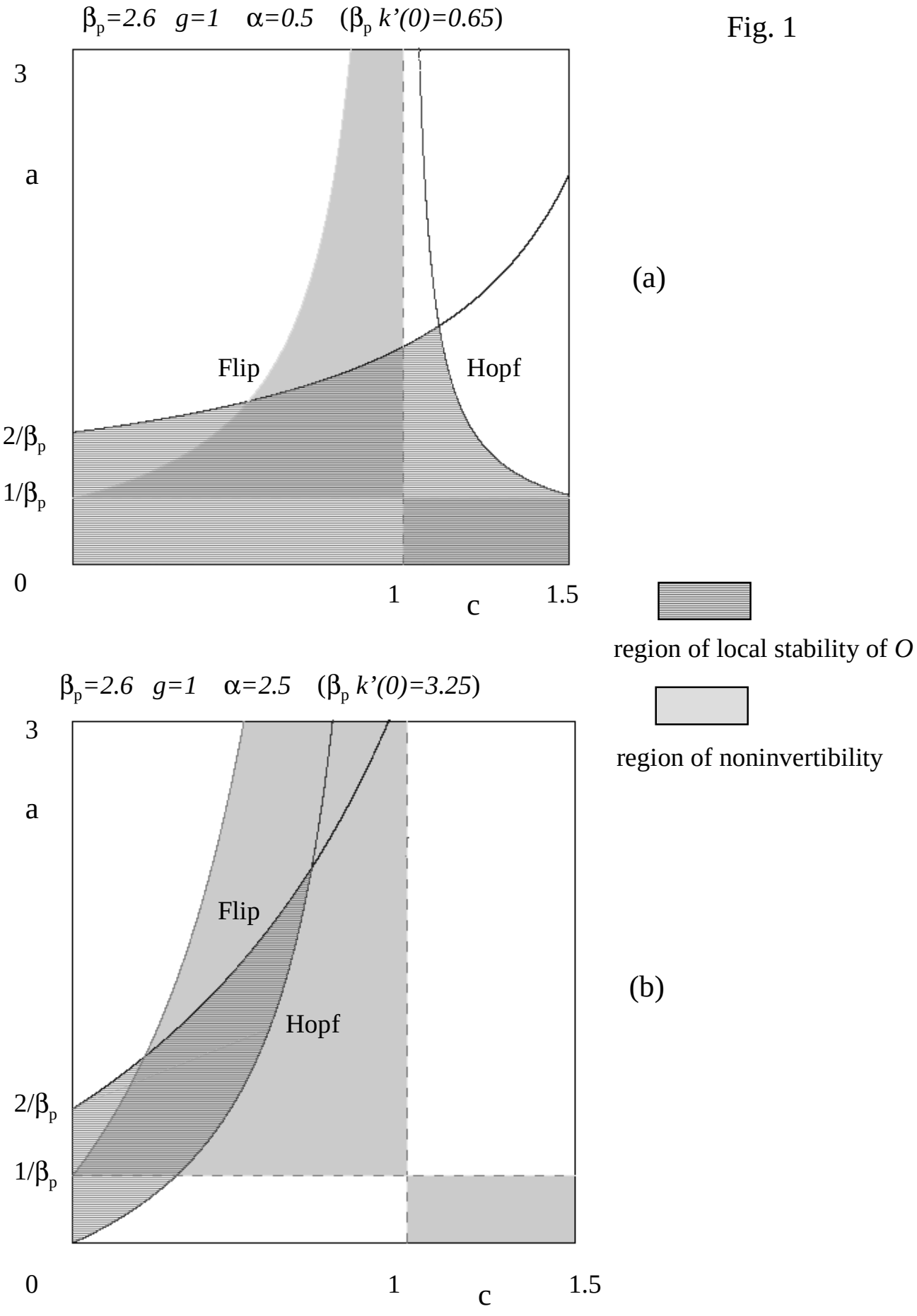
βp=2.6 g=1 α=0.5 (βp k'(0)=0.65)
3
a
Flip
Hopf
2/βp
1/βp
0
1
1.5
c
(a)
region of local stability of O
region of noninvertibility
βp=2.6 g=1 α=2.5 (βp k'(0)=3.25)
3
a
Flip
Hopf
2/βp
1/βp
0
1
1.5
c
(b)

Fig. 2

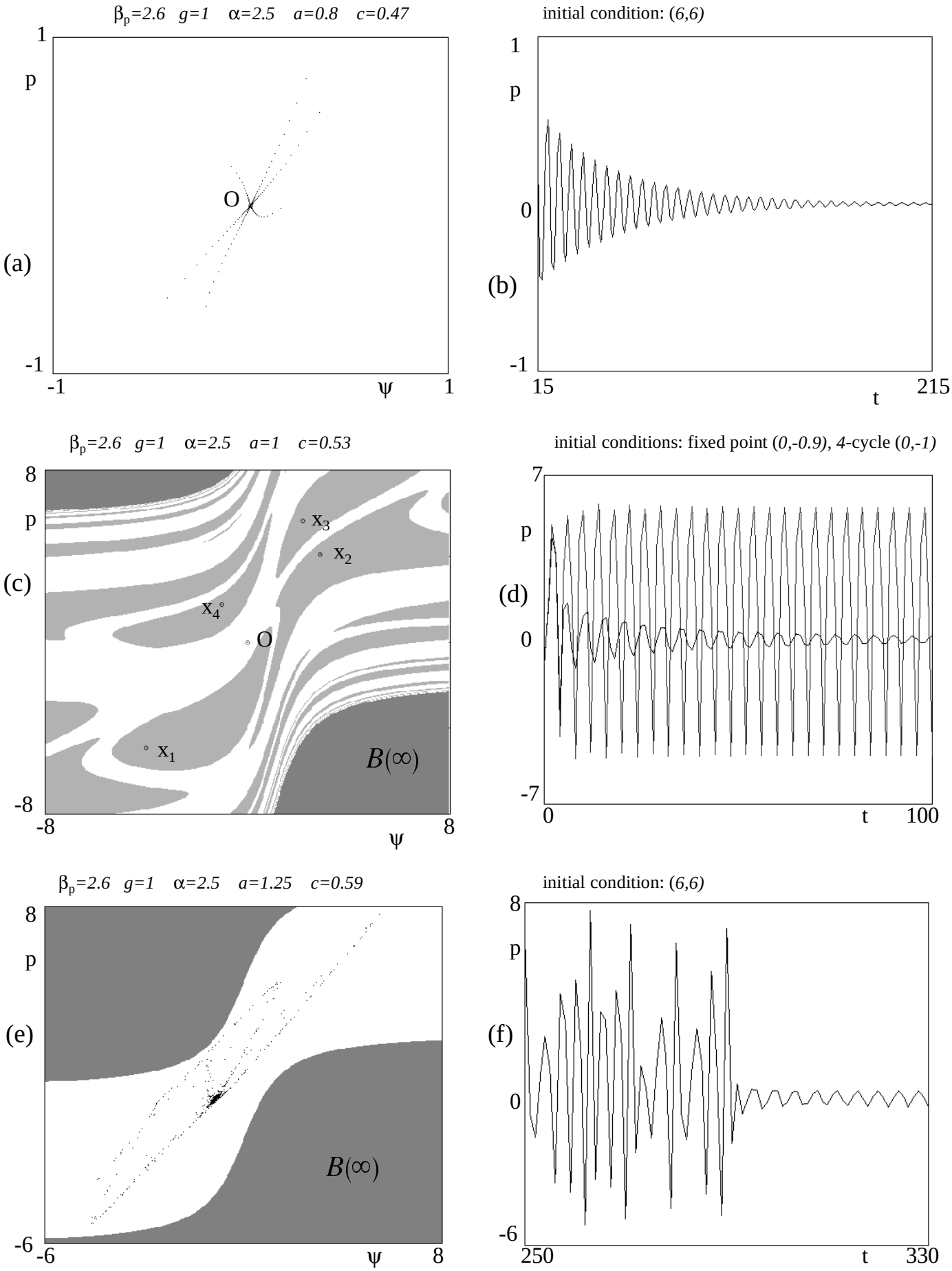
βp=2.6 g=1 α=2.5 a=0.8 c=0.47
initial condition: (6,6)
1
p
O
(a)
-1
-1
ψ
1
1
p
0
(b)
-1
15
t
215
βp=2.6 g=1 α=2.5 a=1 c=0.53
initial conditions: fixed point (0,-0.9), 4-cycle (0,-1)
8
p
x3
x2
(c)
x4
O
x1
B(∞)
-8
-8
ψ
8
7
p
(d)
0
-7
0
t
100
βp=2.6 g=1 α=2.5 a=1.25 c=0.59
initial condition: (6,6)
8
p
(e)
B(∞)
-6
-6
ψ
8
8
p
(f)
0
-6
250
t
330

Fig. 3

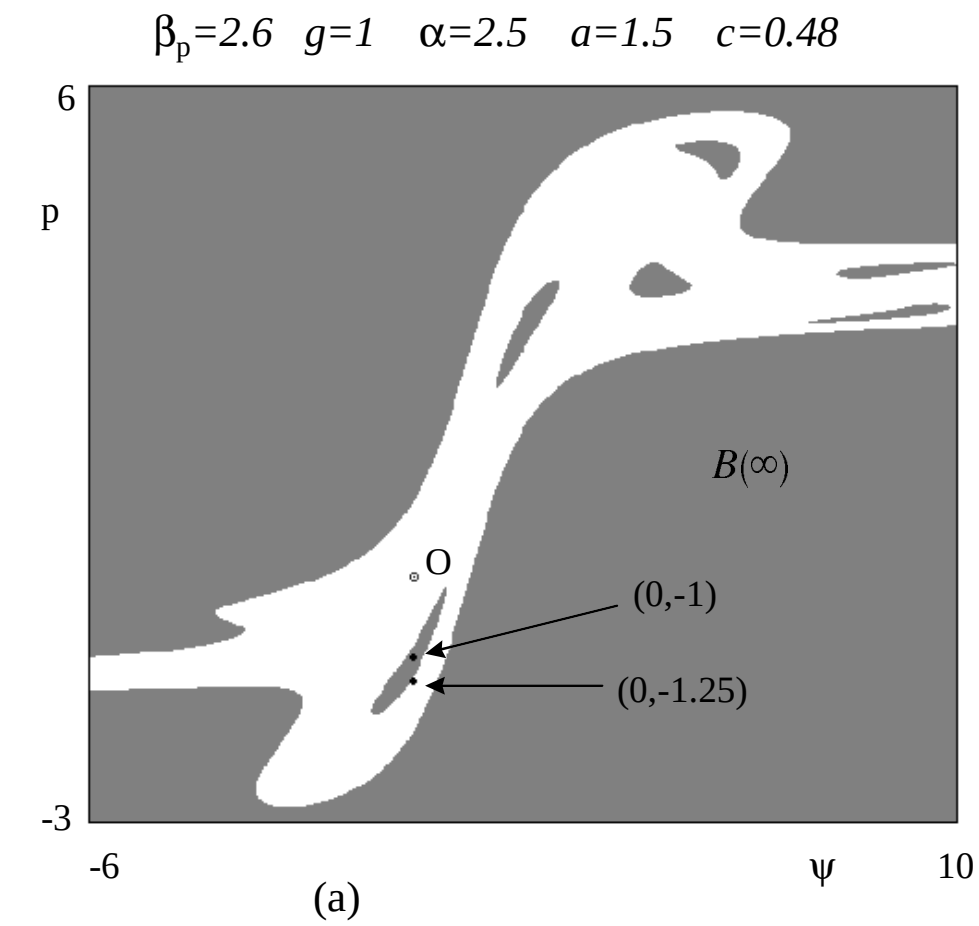
β_p=2.6 g=1 α=2.5 a=1.5 c=0.48
6
p
-3
-6
ψ
10
B(∞)
O
(0,-1)
(0,-1.25)
(a)

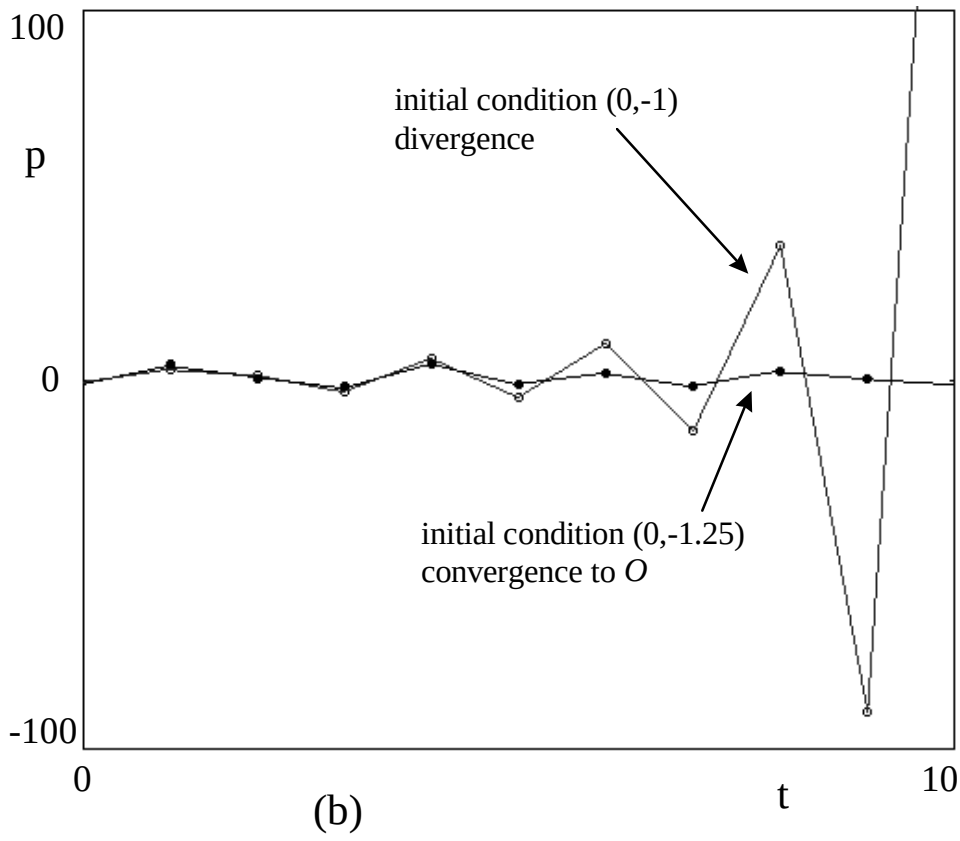
100
p
0
-100
0
t
10
initial condition (0,-1)
divergence
initial condition (0,-1.25)
convergence to O
(b)

Fig. 4

β_p=2.6 g=1 α=2.5 a=0.8 c=0.49

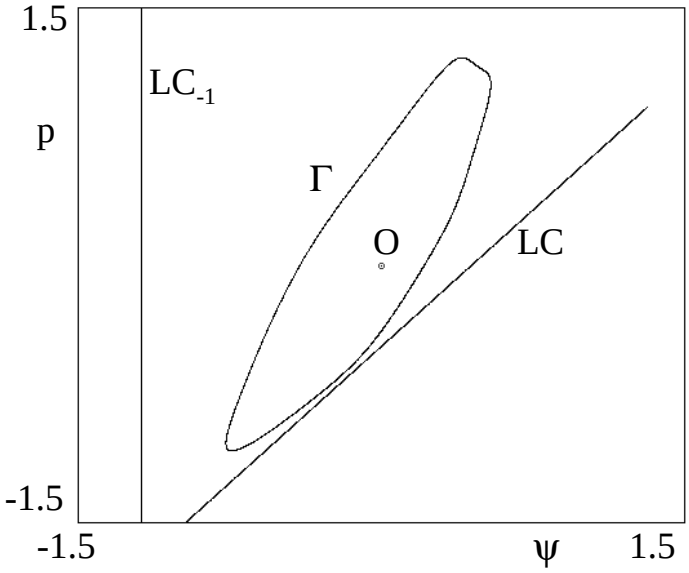

(a)

β_p=2.6 g=1 α=2.5 a=0.8 c=0.52

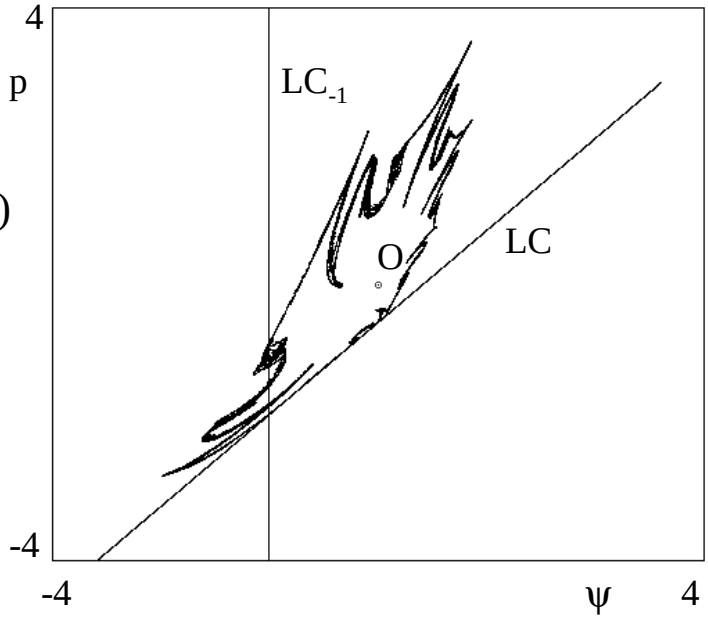

(b)

β_p=2.6 g=1 α=2.5 a=0.8 c=0.6

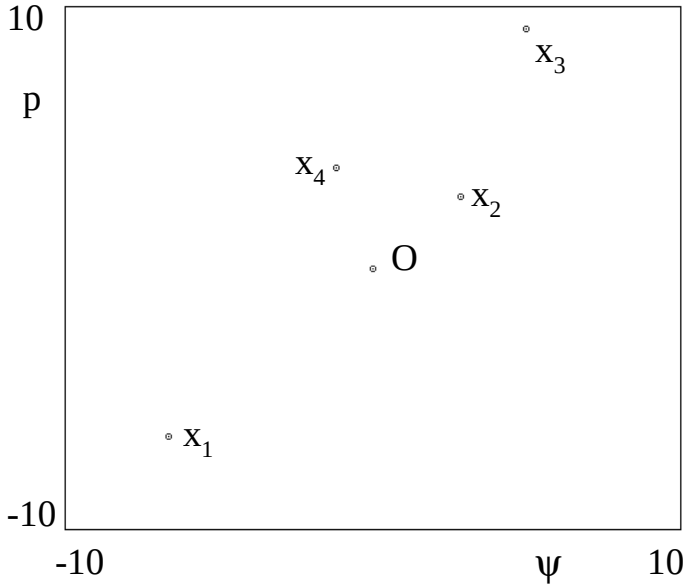

(c)

Fig. 5

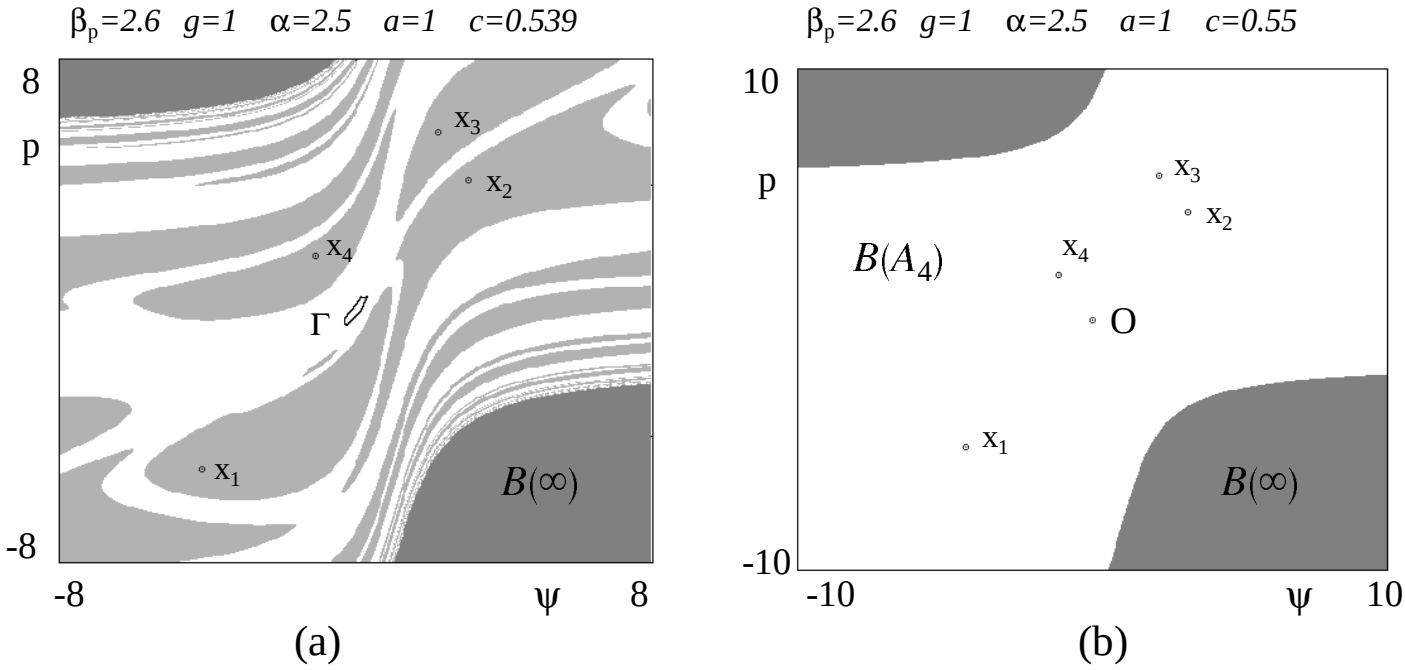
βp=2.6 g=1 α=2.5 a=1 c=0.539
8
p
-8
-8
ψ
8
x3
x2
x4
Γ
x1
B(∞)
(a)
βp=2.6 g=1 α=2.5 a=1 c=0.55
10
p
-10
-10
ψ
10
x3
x2
B(A4)
x4
O
x1
B(∞)
(b)
βp=2.6 g=1 α=2.5 a=1 c=0.69
12
p
-10
-10
ψ
12
O
(c)
βp=2.6 g=1 α=2.5 a=1 c=0.77
12
p
-10
-10
ψ
12
O
(d)

Fig. 6

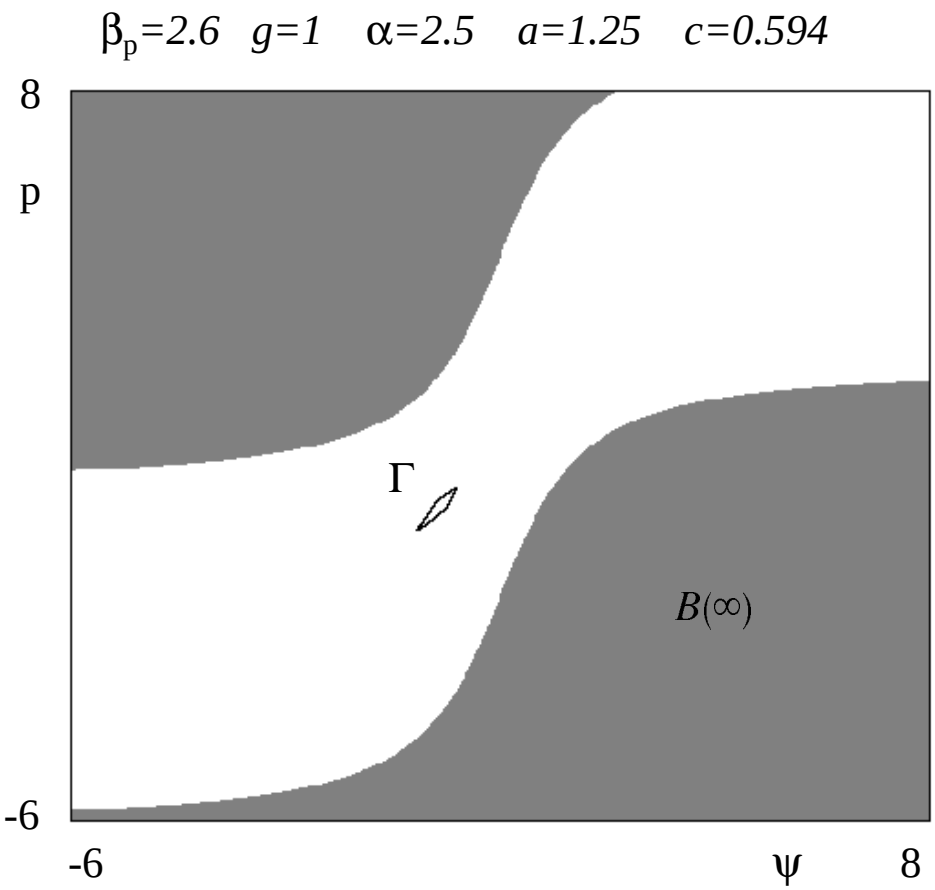
β_p=2.6 g=1 α=2.5 a=1.25 c=0.594
8
p
Γ
B(∞)
-6
-6
ψ
8

(a)

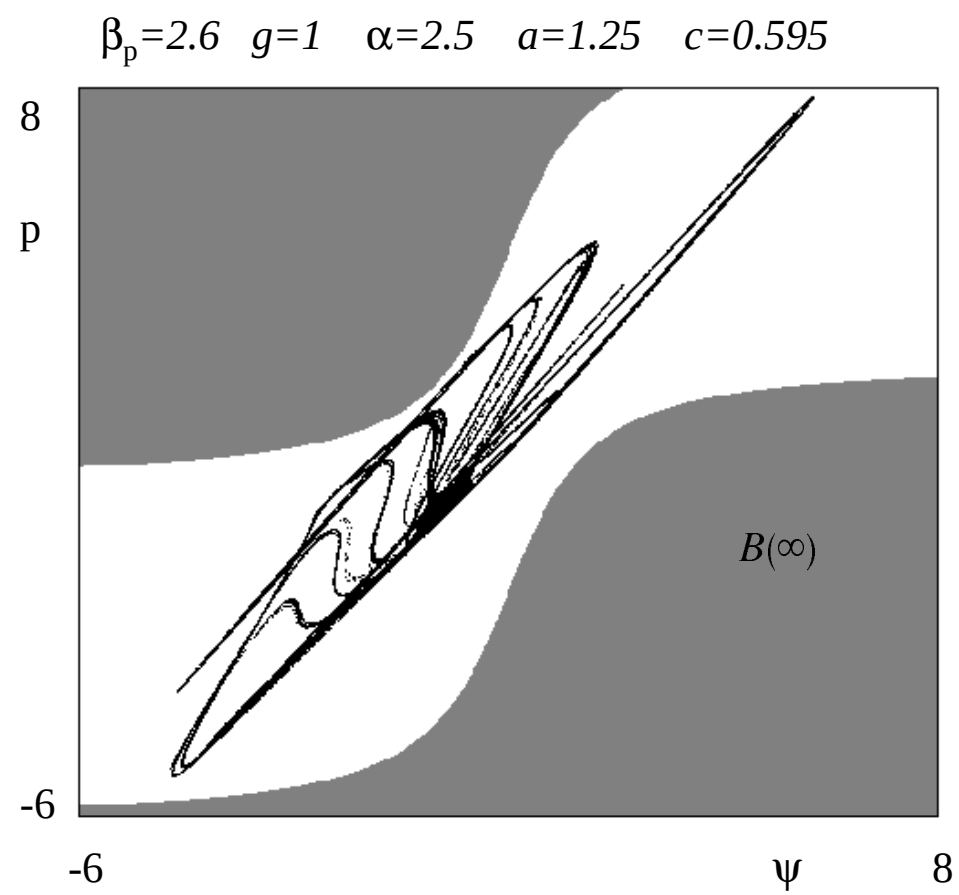
β_p=2.6 g=1 α=2.5 a=1.25 c=0.595
8
p
B(∞)
-6
-6
ψ
8

(b)

Fig. 7

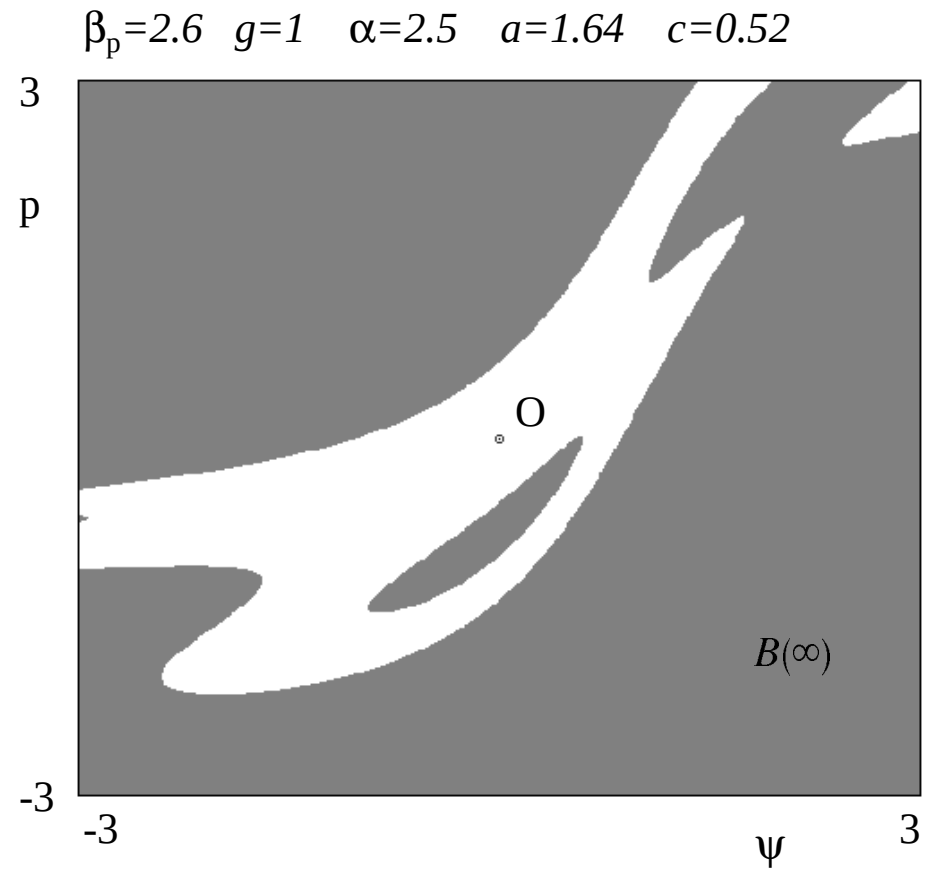
β_p=2.6 g=1 α=2.5 a=1.64 c=0.52
3
p
-3
O
B(∞)
-3
ψ
3

(a)

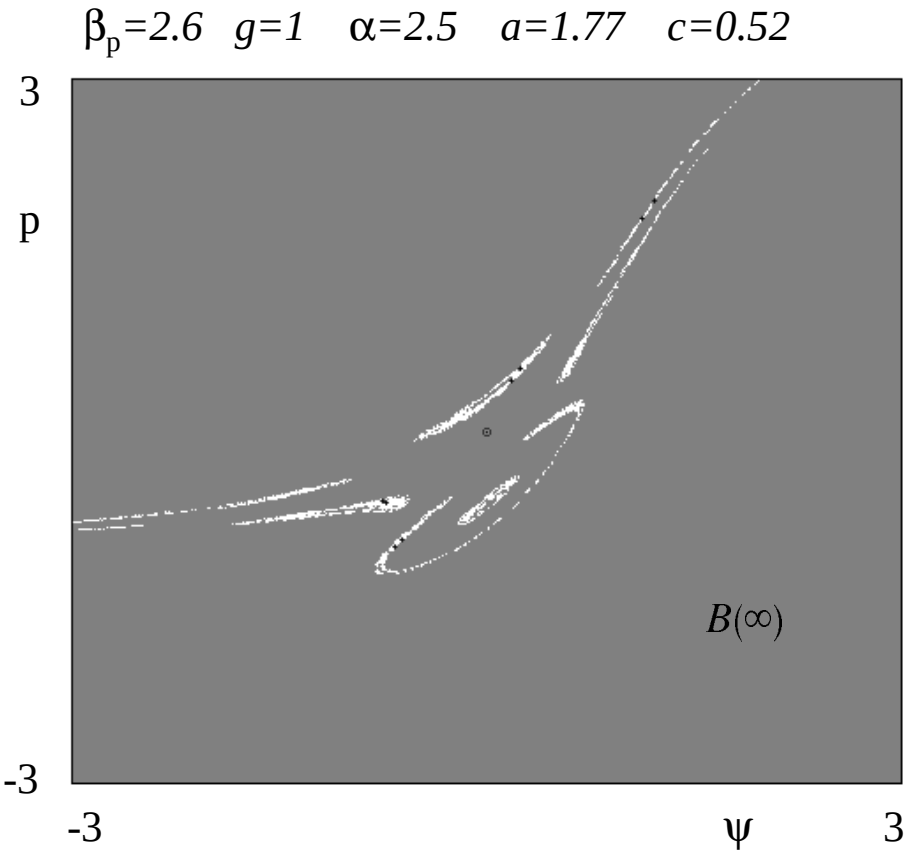
β_p=2.6 g=1 α=2.5 a=1.77 c=0.52
3
p
-3
B(∞)
-3
ψ
3

(b)

Fig. 8

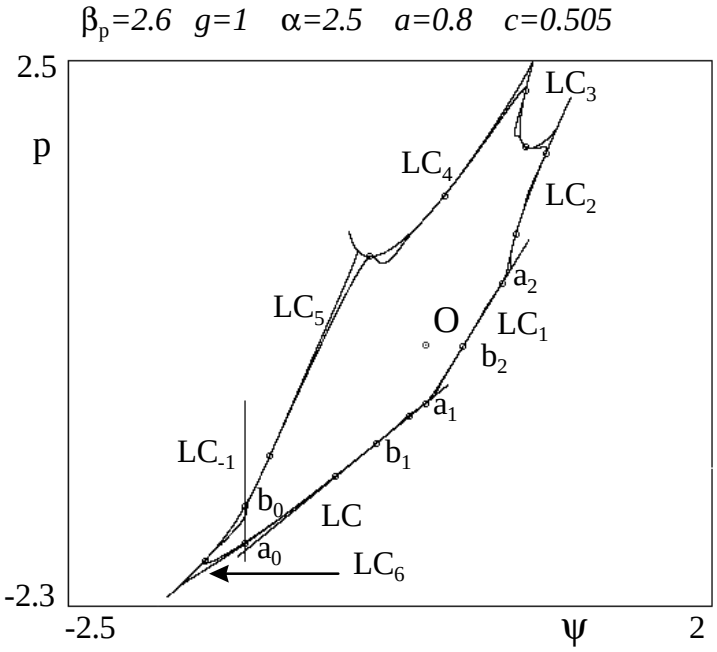

(a)

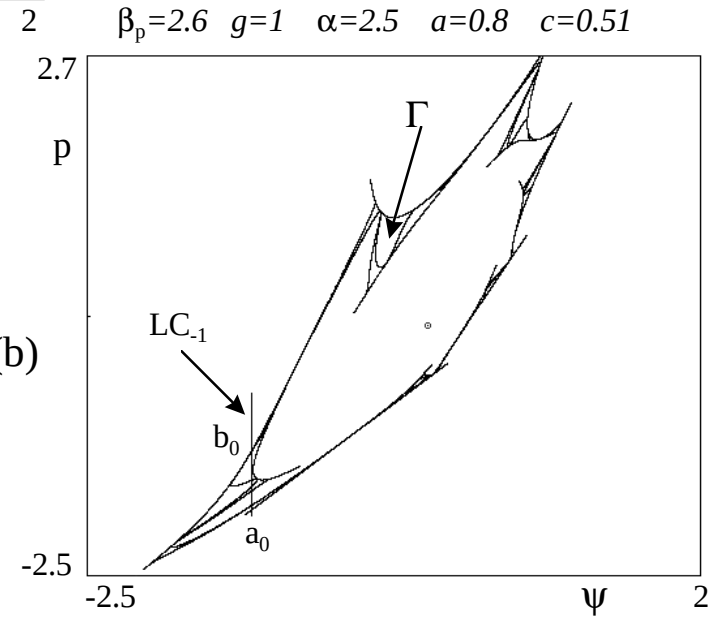

(b)

enlargement of part of the absorbing area

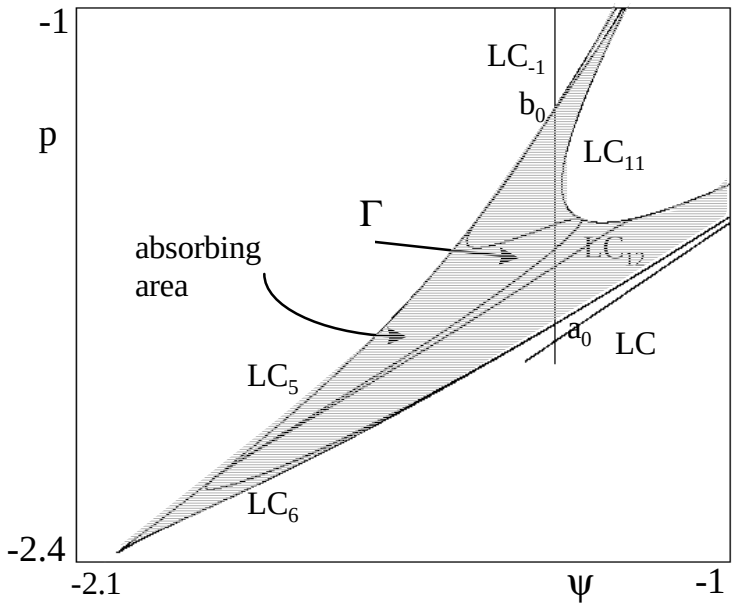

(c)

Fig. 9

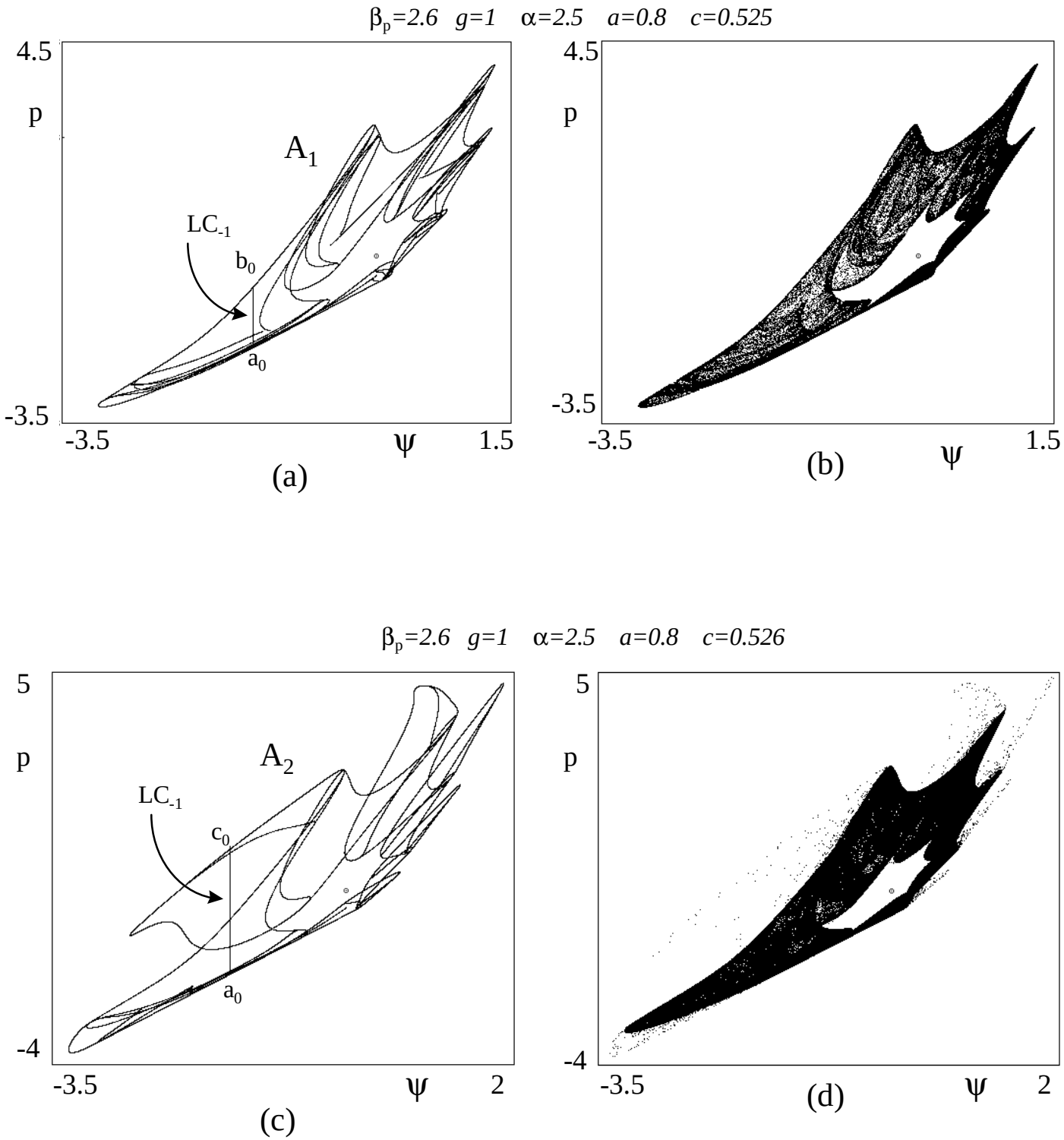
β_p=2.6 g=1 α=2.5 a=0.8 c=0.525
4.5
p
A1
LC-1
b0
a0
-3.5
-3.5
ψ
1.5
(a)
4.5
p
-3.5
-3.5
1.5
ψ
(b)
β_p=2.6 g=1 α=2.5 a=0.8 c=0.526
5
p
A2
LC-1
c0
a0
-4
-3.5
ψ
2
(c)
5
p
-4
-3.5
ψ
2
(d)

Fig. 10

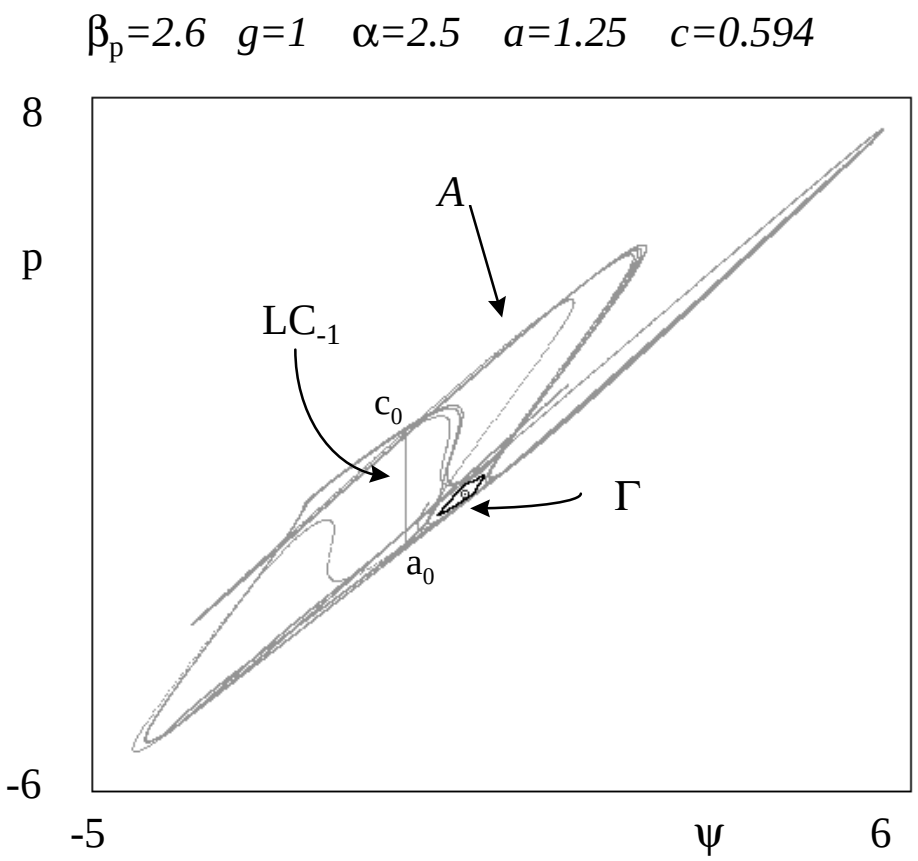

Fig. 11

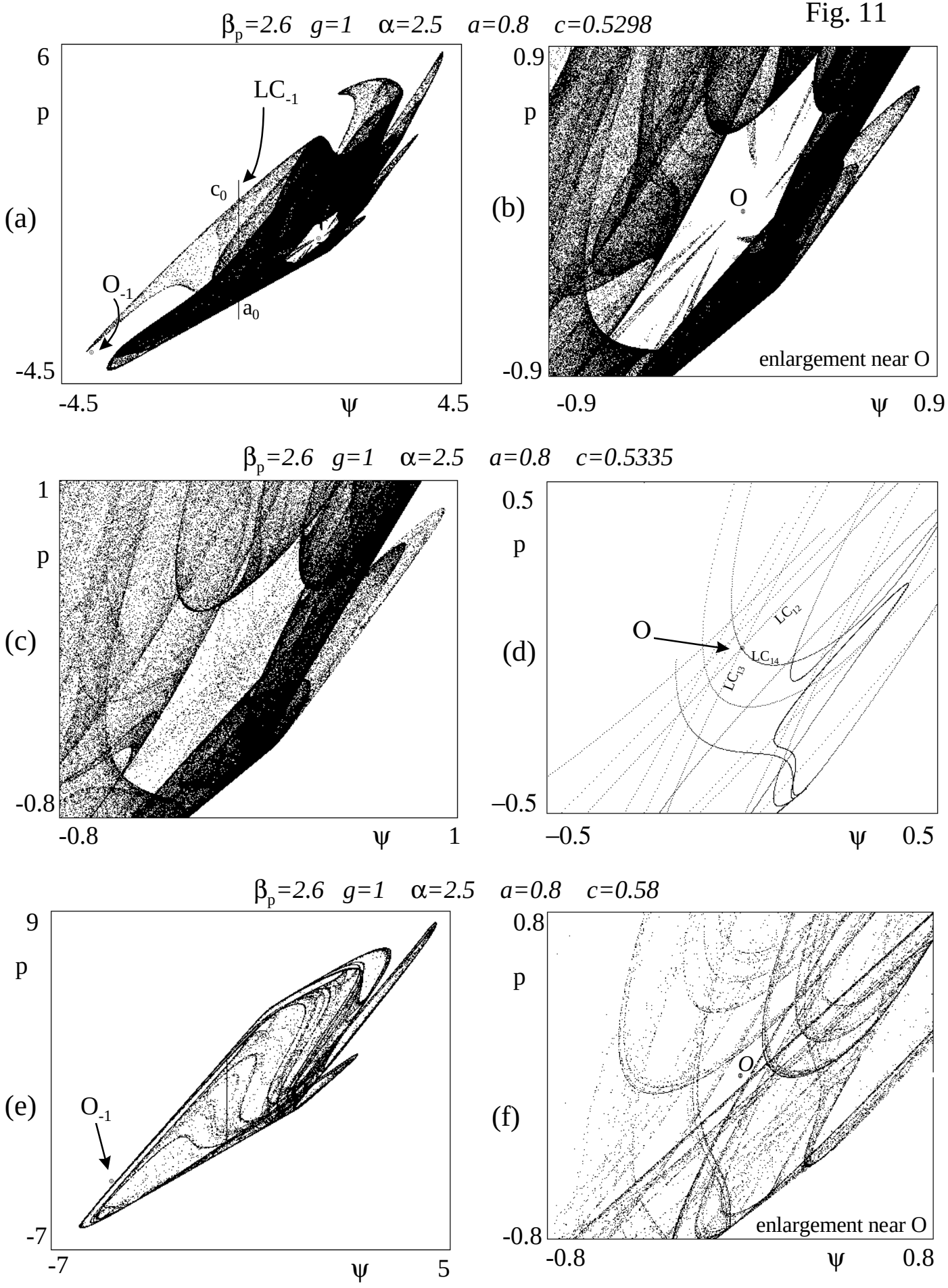
β_p=2.6 g=1 α=2.5 a=0.8 c=0.5298
6
p
LC-1
c0
(a)
O-1
a0
-4.5
-4.5
ψ
4.5
0.9
p
(b)
O
enlargement near O
-0.9
-0.9
ψ
0.9
β_p=2.6 g=1 α=2.5 a=0.8 c=0.5335
1
p
(c)
-0.8
-0.8
ψ
1
0.5
p
(d)
O
LC12
LC14
LC13
–0.5
–0.5
ψ
0.5
β_p=2.6 g=1 α=2.5 a=0.8 c=0.58
9
p
(e)
O-1
-7
-7
ψ
5
0.8
p
(f)
O
enlargement near O
-0.8
-0.8
ψ
0.8

Fig. 12

β_p=2.6 g=1 α=2.5 a=1.25 0.55<c<0.63

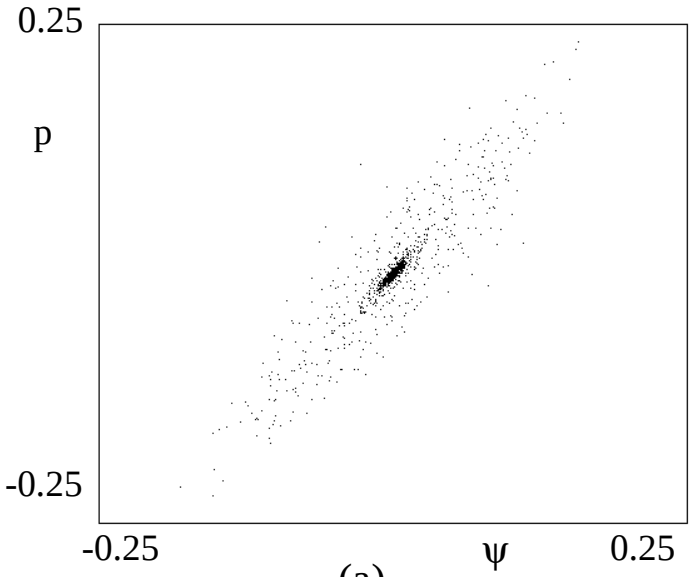

(a)

β_p=2.6 g=1 α=2.5 a=0.8 c=0.49

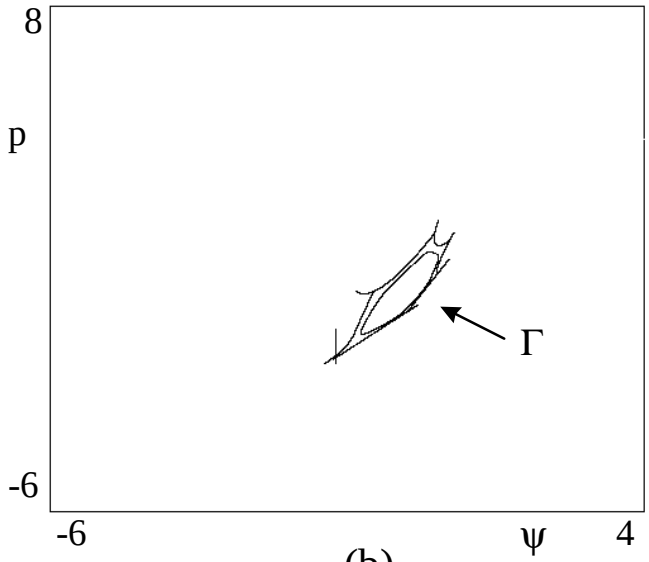

(b)

β_p=2.6 g=1 α=2.5 a=0.8 c=0.55

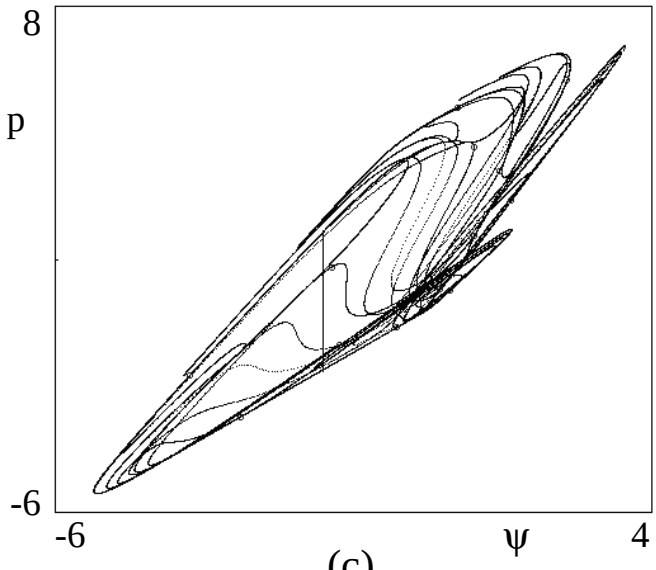

(c)

β_p=2.6 g=1 α=2.5 a=0.8 0.49<c<0.55

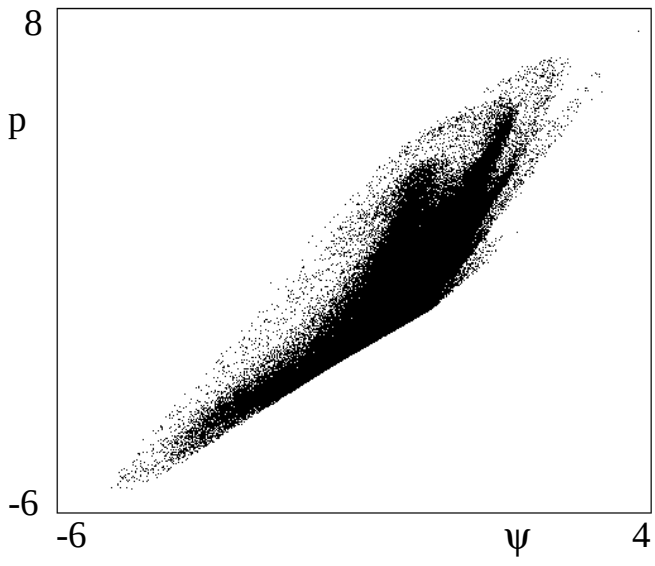

(d)

Fig. 13

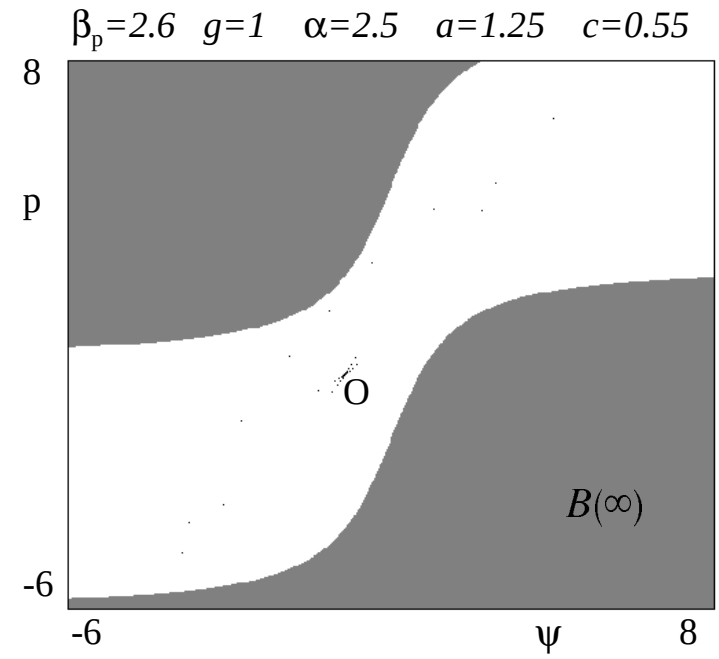
β_p=2.6 g=1 α=2.5 a=1.25 c=0.55
8
p
-6
O
B(∞)
-6
ψ
8

(a)

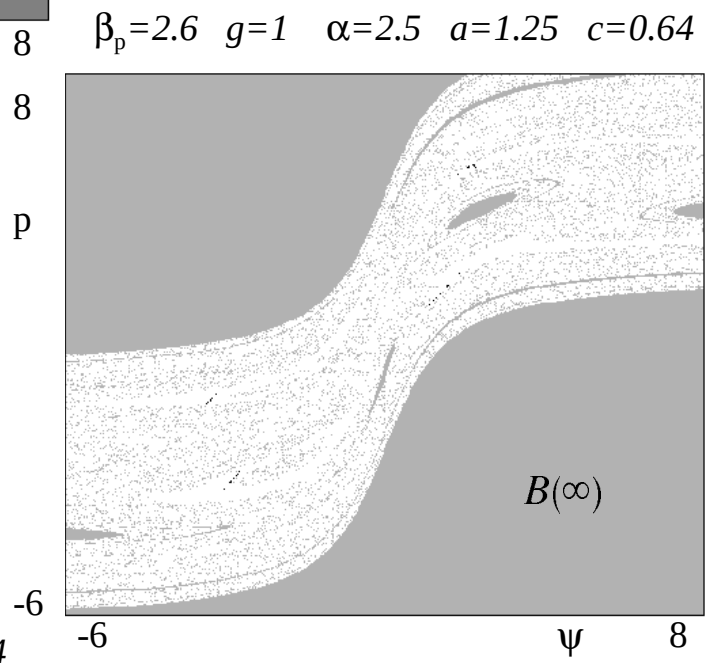
β_p=2.6 g=1 α=2.5 a=1.25 c=0.64
8
p
-6
B(∞)
-6
ψ
8

(b)

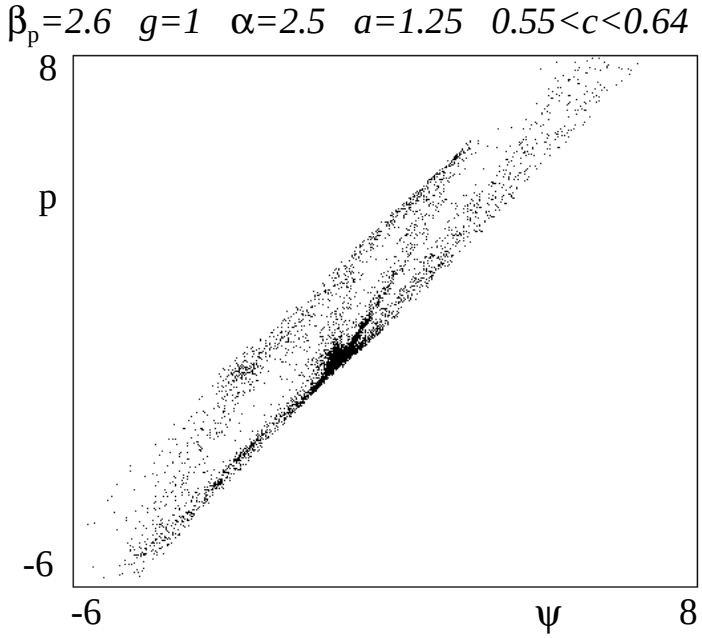
β_p=2.6 g=1 α=2.5 a=1.25 0.55<c<0.64
8
p
-6
-6
ψ
8

(c)